NASA TM X-501

TECHNICAL MEMORANDUM

X-501

A PRELIMINARY INVESTIGATION OF MODIFIED BLUNT 13° HALF-CONE RE-ENTRY CONFIGURATIONS AT SUBSONIC SPEEDS

By George C. Kenyon and George G. Edwards

Ames Research Center
Moffett Field, Calif.

NATIONAL AERONAUTICS AND SPACE ADMINISTRATION
WASHINGTON

March 1961

NATIONAL AERONAUTICS AND SPACE ADMINISTRATION

TECHNICAL MEMORANDUM X-501

A PRELIMINARY INVESTIGATION OF MODIFIED BLUNT 13° HALF-CONE RE-ENTRY CONFIGURATIONS AT SUBSONIC SPEEDS*

By George C. Kenyon and George G. Edwards

SUMMARY

A wind-tunnel study has been conducted to explore methods of modifying a blunt 13° half-cone to provide a re-entry configuration with adequate performance and stability for horizontal landing. The basic 13° half-cone had a maximum lift-drag ratio of 1.7 which was deemed inadequate for horizontal landing. The effects of modifying the aft portion of the blunt half-cone to improve performance, longitudinal stability, and trim characteristics were investigated in some detail. Also evaluated were the incremental effects on the longitudinal aerodynamic characteristics of vertical surfaces, several canopies, a retractable auxiliary lifting surface, control surfaces, and a landing gear. For a preferred combination, performance, stability, and control characteristics were obtained at a Mach number of 0.25 and a Reynolds number of 25 million, essentially full scale. The effects of Mach number on the longitudinal aerodynamic characteristics were studied briefly to a Mach number of 0.9.

The results showed that the rear portion of a 13° blunt half-cone could be contoured to obtain very large increases in lift-drag ratio without large out-of-trim pitching moments. Vertical surfaces, a trailing-edge flap, and elevons all improved the lift-drag ratio. Neither a landing gear nor a canopy on the upper surface had any serious effects on performance or static longitudinal stability provided the canopy did not interfere with the leading-edge vortex system. A complete vehicle configuration had a low-speed, maximum, trimmed lift-drag ratio of over 6 with linear pitching-moment characteristics and positive static longitudinal stability about a moment center at 55 percent of the length. The longitudinal aerodynamic characteristics of this particular configuration were unsatisfactory at high subsonic Mach numbers, but it is believed that these deficiencies could be eliminated with further development.

*Title, Unclassified

INTRODUCTION

In reference 1, it was demonstrated that a lifting body in the form of a blunt 30° half-cone has a hypersonic lift-drag ratio of about 0.5 and suitably adapted as a re-entry vehicle, it would have a lateral range from satellite orbit of the order of 200 miles. Although this low fineness ratio half-cone possesses good lift characteristics at subsonic speeds ($C_{L_{max}} \approx 0.9$ from ref. 2), the high drag resulting from the large, blunt base limits the lift-drag ratio to only 0.9 at landing speeds. Hence, final landing would have to be by parachute or other auxiliary device.

Research on blunt half-cone lifting bodies has been extended to include bodies of increased slenderness which have higher hypersonic lift-drag ratios. Characteristically, these half-cone bodies have lower base area in relation to plan-form area so that improved lift-drag ratios may be anticipated at subsonic speeds as well. Following an analytical study of the hypersonic characteristics of blunt half-cones with half-cone angles ranging from 10° to 20°, one with a 13° angle was selected for detailed experimental studies. Considerations which led to selection of this particular configuration and the results of tests at supersonic speeds in the Ames 10- by 14-Inch Supersonic Wind Tunnel to a Mach number of 5 have been reported in reference 3. This blunt 13° half-cone had a lift-drag ratio of 1.4 at supersonic speeds, indicating that a re-entry vehicle based on this shape would have a lateral range potential in excess of 1000 miles. Concurrent with the tests reported in reference 3, subsonic tests at large scale were conducted in the Ames 12-Foot Pressure Tunnel, the results of which are included in the present report. The maximum lift-drag ratio at subsonic speeds, 1.7, was considerably better than had been measured for a blunt 30° half-cone but was well below the minimum lift-drag ratio of 2.5 suggested in reference 4 to be required for a conventional horizontal landing. Although the pitching-moment variation was nearly linear with lift coefficient, the body was slightly unstable in pitch for a reasonable center-of-gravity position.

The purpose of the present investigation was to study methods by which the basic 13° half-cone could be modified to obtain a re-entry configuration with conventional horizontal landing potential and still retain the good supersonic performance of the basic half-cone. This report presents the results of a preliminary investigation in the Ames 12-Foot Pressure Wind Tunnel to evaluate the effects on performance and stability of body contour, canopy shape, a retractable auxiliary wing, a landing gear, vertical surfaces, and control surfaces in the form of elevons and a trailing-edge flap. Lift, drag, pitching-moment, and base pressure data are presented for all configurations at a Mach number of 0.25 and, for a complete configuration, at Mach numbers from 0.60 to 0.90. The test Reynolds number, based on model length, was 5 million. In addition, longitudinal and lateral data at a Mach number of 0.25 are presented for one complete configuration at a Reynolds number of

25 million, essentially full scale. These results, together with those of reference 3, have been used as the basis for the re-entry configuration based on a blunt 13° half-cone discussed in reference 5.

NOTATION

Coefficients of forces and moments presented are referred to the conventional stability axes for longitudinal data and body axes for lateral data. The moment center for each model was located at 55 percent of the length from the nose and 7 percent of the length below the cone axis. The coefficients and symbols used are defined as follows:

A 3 5 0

b	base diameter
C_D	drag coefficient, $\frac{\text{drag}}{qS}$
C_L	lift coefficient, $\frac{\text{lift}}{qS}$
C_l	rolling-moment coefficient, $\frac{\text{rolling moment}}{qbS}$
C_m	pitching-moment coefficient, $\frac{\text{pitching moment}}{q\ell S}$
C_{m_o}	pitching-moment coefficient at zero lift
C_n	yawing-moment coefficient, $\frac{\text{yawing moment}}{qbS}$
C_p	base-pressure coefficient, $\frac{p_b - p}{q}$
C_Y	side-force coefficient, $\frac{\text{side force}}{qS}$
i_w	angle of incidence of wing, measured from cone axis
$\frac{L}{D}$	lift-drag ratio, $\frac{\text{lift}}{\text{drag}}$
ℓ	model length
M	free-stream Mach number
p	free-stream pressure

p_b base pressure

q free-stream dynamic pressure

R Reynolds number, based on model length

r leading-edge radius

S body plan-form area

α angle of attack, referenced to cone axis

β angle of sideslip

δ_e elevon deflection, positive with leading edge up, measured from plane parallel to cone axis

δ_f trailing-edge flap deflection, positive with trailing edge down, measured from tangent to upper surface at the base

δ_{wf} auxiliary wing flap deflection, positive with leading edge up

A 3 5 0

MODELS

The geometric properties of the various models and components are given in figures 1 through 8 and photographs of some of the models are presented in figure 9. Figures 1 through 4 delineate the four body shapes referred to herein as bodies 1, 2, 3, and 4, respectively. These bodies were developed from one basic structure by providing a horizontal parting plane on the cone axis and another normal to the cone axis near the rear of the model to permit replacement of the top and rear sections. The models were constructed of wood fitted around a steel inner structure that incorporated a mounting for the six-component strain-gage balance. An orifice for measuring base pressure was located just inside the balance cavity, adjacent to the sting. The models were painted with lacquer and hand rubbed with No. 400 sandpaper to a smooth finish. The wing (figs. 7 and 9(c)) was constructed of aluminum.

If the models were considered to be 1/6 scale, the full-scale vehicle would match the upper stage of a booster with 10-foot diameter. The nose radius, 3 inches for all models, would be 1-1/2 feet full scale. Such a vehicle would be large enough to permit side-by-side seating for two men. The complete configuration (fig. 9(e)) consisted of body 4 with vertical surfaces, elevons, trailing-edge flap, and canopy A. Details of these components along with the landing gear and ventral fin are given in figure 5. Details of canopies B, C, and D are given in figure 8. The wing (figs. 7 and 9(c)) had an NACA 4412 section and was equipped with

a 0.25-chord plain trailing-edge flap. Geometric properties of the wing are shown in figure 7. Details of a fairing added to the upper surface to improve the high-speed characteristics of the configuration are shown in figure 6. This fairing extended the flat portion of the upper surface all the way to the rear of the model, approximating the upper surface of the basic 13° half-cone.

Some additional details concerning the four bodies (figs. 1 through 4) are as follows:

Body 1 (fig. 1) was the basic blunt half-cone configuration, identical to that reported in reference 3, from which other configurations of the present investigation were derived. Body 1 was basically a blunt 13° half-cone with a spherical nose. However, to provide a radius upper leading edge and additional volume, the flat upper surface extended above the cone axis and was inclined relative to the axis. The body was provided with upper plates with edge radii of 0.6 inch, 1 inch, 1.4 inches, 1.73 inches, and one with edge radius that varied from 1.4 inches at the nose to 0.6 inch at the base. In all cases the height of the top surface above the cone axis at the base was constant at 1.73 inches so that the angle of the top surface relative to the cone axis changed with a change in edge radius. These angles were, respectively, 2.0°, 1.3°, 0.5°, 0°, and 0.5°. The base area was 47.2 percent of the plan-form area.

Body 2 (fig. 2) was a modification of body 1 incorporating a small amount of boattailing of the conical surface and curvature of the rear third of the upper surface. The base area was 31.2 percent of the plan-form area or about two-thirds that of body 1. As may be seen in figure 9(c), the space left by cutting away the upper surface could provide a shielded position for a retracted auxiliary wing.

Body 3 (fig. 3) was 6 inches longer than bodies 1 and 2 to provide an extended boattail. Curvature of the upper surface and the boattail resulted in a base area less than half that of body 1, or 17.5 percent of the plan-form area. Cross sections of the lower surface were circular.

Body 4 (fig. 4) was derived on the basis of results obtained with bodies 1, 2, and 3. The body was 4 inches longer than bodies 1 and 2. Curvature of the upper surface was started farther forward than on body 3 in an attempt to move the center of pressure forward and improve the pressure recovery at the base. Curvature of the lower surface was also started farther forward and the radius increased to improve pressure recovery over the bottom surface at low angles of attack as a means of making C_{m_0} more positive. Cross sections of those lower surfaces that departed from the conical surfaces of body 1 were elliptical rather than circular as for body 3. The upper edge radius was variable, with a radius of 1.4 inches at the nose, and reduced radii aft to the vertical surfaces that were added later. The base area of body 4 was 17.1 percent of the plan-form area.

TESTS

Longitudinal Tests

Low speed.- Bodies 1 through 4 were tested at a Mach number of 0.25 and a Reynolds number of 5 million through an angle-of-attack range from -16° to $+24^{\circ}$. Lift, drag, pitching moment, and base pressure were measured. Bodies 1, 2, and 3 were also tested with the auxiliary wing, and body 4 was tested with various canopies, control surfaces, and landing gear.

Body 1 (the basic 13° blunt half-cone) and a complete configuration utilizing body 4 were also tested at Mach number 0.25 and Reynolds number 25 million. This Reynolds number was achieved by operating the wind tunnel at a stagnation pressure of 5 atmospheres. Hence, if models are considered to be 1/6 scale, a Reynolds number of 25 million was nearly full scale. These tests included measurements of the effectiveness of the trailing-edge flap and of the elevons.

High speed.- A complete re-entry configuration, consisting of body 4, canopy A, vertical surfaces, elevons, and a trailing-edge flap, was tested at Mach numbers of 0.60, 0.70, 0.80, 0.85, and 0.90 at a constant Reynolds number of 5 million. The angle-of-attack range was -10° to $+16^{\circ}$. Similar tests were performed with a fairing added to the upper aft surface of the configuration (fig. 6).

Lateral-Directional Tests

Six-component force data were obtained for the complete re-entry configuration, with and without a ventral fin, for a range of sideslip angles from -10° to $+16^{\circ}$ at a constant angle of attack of 6°. With the ventral fin added, similar data were obtained for constant angles of attack of -6°, 0°, and $+12^{\circ}$. These tests were performed at a Mach number of 0.25 and a Reynolds number of 25 million.

CORRECTIONS TO DATA

The data have been corrected for constriction effects due to the presence of the tunnel walls. Calculations of the tunnel-wall interference originating from lift on the model show this effect to be negligible. The angle of attack was corrected for the deflection of the sting due to aerodynamic loads.

The corrections due to constriction effects were made according to the method of reference 6. The corrections to the dynamic pressure and the corresponding Mach number are listed on the following table:

Corrected Mach number	Uncorrected Mach number	$\frac{q_{corrected}}{q_{uncorrected}}$
0.25	0.25	1.003
.60	.598	1.004
.70	.698	1.005
.80	.795	1.008
.85	.843	1.010
.90	.888	1.015

Since a gliding flight is being considered, the drag measurements were not corrected for the base pressure. The sting, with a diameter of 2-1/2 inches, was small in comparison with the model base, and it is believed, therefore, that sting interference effects were negligible.

RESULTS AND DISCUSSION

The Basic Blunt 13° Half-Cone (Body 1)

The basis for selection of a blunt 13° half-cone as a study configuration has been presented in reference 3 and reviewed in the Introduction to this report. The present investigation began with an assessment of the horizontal landing potential of this basic configuration. The static longitudinal aerodynamic characteristics of body 1, the basic blunt 13° half-cone, are presented in figure 10 for a Mach number of 0.25 and two Reynolds numbers, 5 million and 25 million. Pitching moments are referred to a point 55 percent of the length of the body aft of the nose and 7 percent of the length below the cone axis. The maximum lift-drag ratio of 1.7 was much too low to permit a horizontal landing (see ref. 4). The configuration lacks longitudinal stability but the relatively linear lift and pitching-moment curves were both surprising and encouraging. Base pressure recovery was poor (see fig. 10) and this, together with the fact that the base area was 47 percent of the plan-form area, accounts in large part for the high drag and low lift-drag ratio. Figure 10 shows also the small Reynolds number effects on the forces and moments in the range from 5 million to 25 million. Increasing the Reynolds number did, however, increase the base pressure recovery appreciably at the higher lift coefficients.

The effects of increasing the leading-edge radius of the upper surface were briefly investigated. The results, shown in figure 11, indicate

practically no effect on the lift-drag ratio but some increase in longitudinal stability at the higher lift coefficients as the leading-edge radius was increased.

Effects of Body Modifications (Bodies 2, 3, and 4)

Boattailing is a well-known method of reducing base area and increasing the base pressure coefficient of bodies of revolution, although its application to the unsymmetrical half-cone lifting body does not appear to have been studied in detail. By virtue of the asymmetry of the half-cone, variations in the amount and longitudinal extent of the boattailing on the conical surface as compared to that of the flat upper surface produce camber effects which alter the angle of zero lift and the center of pressure as well as reduce the base drag. The sequence of modified bodies represented by bodies 2, 3, and 4 (figs. 2, 3, and 4, respectively) incorporated several types and amounts of boattailing. The low-speed static longitudinal aerodynamic characteristics of bodies 2, 3, and 4 are compared with those of the basic blunt 13° half-cone (body 1) in figure 12. Moments are referred to a point 55 percent of the length of each individual body aft of the nose and 7 percent of the length below the cone axis. Base pressure coefficients for these bodies are shown as a function of lift coefficient in figure 13.

The rear part of the upper surface of body 2 was curved downward, and only a small amount of boattailing was applied to the conical surface. The large positive camber effect is evident in the data of figure 12 which indicates large negative shifts in the angle for zero lift and in the pitching moments throughout the angle-of-attack range as compared to the basic body 1. The reduced base area of body 2 and improved pressure recovery at the base (shown in fig. 13) produced a large improvement in lift-drag ratio.

Body 3 had an extended afterbody with more boattailing applied to the conical surface for the purpose of reducing positive camber and obtaining a further reduction of base area. As expected, the angle of zero lift and the pitching moments were shifted in a positive direction as compared to those of body 2 (fig. 12). A point of interest in these data is an apparent change in flow characteristics at about 0° angle of attack. At this angle, the data show an increase in lift-curve slope, a rearward shift in the aerodynamic center, and a sudden downward trend in L/D with lift coefficient. These changes apparently were related to the development of a strong vortex pair emanating from the edges of the body. The effects of this vortex on a tuft grid placed at the base of body 3 are shown in figure 14. Tuft and oil flow studies on the sharply curved upper surface showed strong outflow into the vortex system.

Body 4 incorporated further changes in the boattail, designed to produce a more positive C_{m_0}. Compared with body 3, the amount and extent

of boattailing on the conical surface were increased while curvature of the upper surface was reduced. These changes resulted in only a small change in the ratio of base area to plan-form area (from 17.5 to 17.1 percent), but there was a large improvement in L/D as shown in figure 12. This figure also shows a large positive shift in C_{m_o} as compared with body 3. The angle of zero lift and the lift-curve slope were about the same as for the basic half-cone, body 1. The base pressure recovery was only slightly less than for body 3 (fig. 13).

Effects of an Auxiliary Lifting Surface

Through the early part of this investigation, some experiments were performed to determine the aerodynamic effects of an auxiliary lifting surface for augmenting the lifting characteristics of modified blunt half-cones. The auxiliary wing, shown in figures 7 and 9(c), was proportioned so that it could be retracted and shielded during the heating phase of re-entry. Bodies 1, 2, and 3 were tested with the wing. Wing incidence, wing position, and flap angle were variables. The results presented in figures 15, 16, 17, and 18 show, in general, improvements in lift-drag ratio at the higher lift coefficients and considerable reduction in the angle of attack to attain a given lift coefficient. Offsetting these gains to some extent were the large out-of-trim pitching moments resulting from a rearward shift in the center of pressure. The utility of such an auxiliary lifting surface, weighed against the probable attendant weight penalty and structural problems as well as operational complexities, did not appear to overcome the disadvantages associated with its use.

Effects of Various Appendages and Canopies on Longitudinal Aerodynamic Characteristics

Figure 19 shows the effects of adding vertical surfaces and a spherical-segment type of canopy (canopy B) to body 4. The vertical surfaces produced end-plate effects which reduced the drag at positive angles of attack and increased the lift-curve slope slightly, resulting in improvement of the lift-drag ratio. Observations of the tuft grid shown in figure 14 indicated that the vertical surfaces constrained the vortex pair emanating from the leading edges, forcing the air from the vortices into the boundary layer on the curved surface, and thereby alleviating separation. There was a negative shift in pitching moment as a result of increased lift on the curved upper surface. The addition of the spherical-segment canopy reduced the lift-drag ratio and led to some further experiments on the effects of canopy shape. The results of these tests are discussed below.

The effects of a constant-chord trailing-edge flap and elevon control surfaces are shown in figure 20. The geometric characteristics of these appendages are given in figure 5. Both types of surface improved the lift-drag ratio and static longitudinal stability.

Figure 21 presents a comparison of the effects of four different canopies on the pitching-moment characteristics and lift-drag ratios of body 4 with vertical surfaces, trailing-edge flap, and elevons. Canopy B is the spherical-segment canopy previously mentioned. Canopy A consisted of canopy B with a cylindrical rear fairing of the same radius (see fig. 5). Canopy C had elliptical sections normal to the plane of symmetry (see fig. 8(a)). Canopy D (fig. 8(b)) was an attempt to blend the canopy into the body to improve aerodynamic efficiency and increase body volume. Figure 21 shows that the model with canopy A had the highest lift-drag ratio of the group and an essentially linear pitching-moment characteristic. It is noted that canopy D caused a drastic reduction in lift-drag ratio and a sudden loss in longitudinal stability at a lift coefficient of slightly over 0.4. This faired canopy, extending to the leading edge, interferred with the strong vortex flows that originate at the leading edges of the upper surface. Tuft studies indicated that the loss of performance and the longitudinal instability occurred when the vortices were diverted outward by the canopy and impinged on the vertical surfaces and elevons.

The incremental effects of a landing gear on the longitudinal characteristics were small as can be seen in figure 22. This landing gear consisted of a pair of skids and a nose wheel (see fig. 5).

Low-Speed Aerodynamic Characteristics of a Complete Vehicle Configuration

The foregoing discussion has indicated the basis for selection of a vehicle configuration suitable for further study to establish whether a modified blunt 13° half-cone, without a wing but with suitable appendages, can satisfy the aerodynamic requirements for a conventional horizontal landing. The selected configuration utilized body 4, canopy A, the vertical surfaces, the trailing-edge flap, and the elevons. The landing gear was omitted.

The initial results obtained at a Reynolds number of 5 million were extended to 25 million. The static longitudinal aerodynamic characteristics of the complete configuration at these two Reynolds numbers are compared in figure 23. Although the effects of increasing Reynolds number in this range are indicated to be small, they were favorable in all respects. Data for the basic blunt 13° half-cone (body 1) are repeated for comparison.

The effects of elevon and flap deflection on the static longitudinal aerodynamic characteristics are presented in figure 24 for a Mach number of 0.25 and a Reynolds number of 25 million. The data show that the configuration was longitudinally stable, that the pitching-moment curves were nearly linear, and that the configuration could be trimmed through a considerable range of lift coefficients with the trailing-edge flap. However, this flap would probably be ineffective as a trim control at high Mach numbers. Figure 24 also shows that the elevons were effective as longitudinal trim controls. With regard to lift-drag ratios shown in figure 24, it is noted that maximum trimmed lift-drag ratios were about 6 but that they occurred at lift coefficients slightly above 0.2. The lift-drag ratio was 3 at a trimmed lift coefficient of about 0.6. In the light of the conclusions of reference 4, indicating a minimum value of 2.5 for attaining a horizontal landing, the results indicate that adequate performance can be obtained. The landing would be made on the back side of the L/D curve for a vehicle of this type (estimated wing loading, 60 lb/sq ft), but according to reference 7, this is perhaps acceptable since the vehicle is longitudinally stable. An extension of the present investigation, reported in reference 5, has indicated further modifications of the body and control surfaces to attain controllability throughout the speed range, to increase the lift coefficient for $(L/D)_{max}$, and to reduce the gradient of L/D with lift coefficient above $(L/D)_{max}$.

The static lateral-directional characteristics were evaluated at a Mach number of 0.25 and a Reynolds number of 25 million. The model had low directional stability, indicating inadequate vertical surfaces. A ventral fin having the dimensions shown in figure 5 was added to improve directional characteristics. A comparison of results for the configuration with and without the ventral fin is presented in figure 25 for a range of sideslip angles at a constant angle of attack of 6°. The ventral fin increased the directional stability but did not eliminate the sudden loss of directional stability that occurred at a sideslip angle of about 8°. At this combination of angle of attack and sideslip, the vortices emanating from the edges of the body apparently were impinging on the vertical surfaces. Lateral-directional characteristics of the configuration with ventral fin were also measured at constant angles of attack of -6°, 0°, and $+12^{\circ}$ for a range of sideslip angles. These results, presented in figure 26, show that the configuration had directional stability and positive dihedral effect; also, that the curves are essentially linear except as previously indicated for the 6° angle-of-attack condition.

Effects of Mach Number on the Longitudinal Aerodynamic Characteristics

A limited investigation of the longitudinal aerodynamic characteristics of the complete re-entry configuration to a Mach number of 0.90 indicated deterioration in these characteristics above a Mach number of 0.70. The

difficulty was believed to be associated with the occurrence of local supersonic flow on the upper surface in the curved region behind the canopy. A fairing was added to eliminate the curvature in the upper surface, as shown in figure 6. On a full-scale vehicle, this could be a "blow-away" fairing or a modulated surface. Comparisons of the longitudinal aerodynamic characteristics, with and without the fairing, are presented in figure 27. The fairing reduced the effective camber in the configuration, resulting in a large forward movement of the center of pressure and large positive pitching moment at zero lift. Abrupt changes in pitching moment were alleviated by the fairing at Mach numbers of 0.85 and 0.90 and stability was somewhat improved. Below a Mach number of 0.85, the configuration with the fairing had discontinuities in the lift and pitching-moment curves at a lift coefficient of about 0.2. At all Mach numbers, the fairing drastically reduced the lift-drag ratio, although this is perhaps not serious in this transient speed regime of a re-entry vehicle.

It is concluded that the configuration would require further investigation and modifications to attain satisfactory longitudinal aerodynamic characteristics at high subsonic Mach numbers.

CONCLUSIONS

A wind-tunnel study has been conducted to explore methods of modifying a blunt 13° half-cone to provide a re-entry configuration with adequate performance and stability for horizontal landing with the following conclusions:

1. The basic blunt 13° half-cone had a low-speed lift-drag ratio of only 1.7 but nearly linear lift and pitching-moment characteristics. It was demonstrated that by proper reshaping of the rear part of the half-cone, large improvement in lift-drag ratio can be obtained without large out-of-trim pitching moments.

2. Experiments with a retractable auxiliary lifting surface mounted above the body showed considerable improvement of the lift-drag ratio, at the higher lift coefficients, over those of the body alone and a reduction in the angle of attack to obtain a given lift coefficient. These improvements were accompanied by relatively large out-of-trim pitching moments.

3. Vertical surfaces, a trailing-edge flap, and elevons all improved the lift-drag ratio. The addition of a landing gear and canopy had little effect on the longitudinal aerodynamic characteristics of the model provided the canopy did not interfere with the leading-edge vortex system.

4. A complete vehicle configuration, consisting of a modified blunt 13° half-cone, a canopy, vertical surfaces, and longitudinal controls, was shown to have low-speed lift-drag ratios ranging from 6 at a trimmed lift coefficient of 0.2 to 3 at a trimmed lift coefficient of 0.6. The configuration had nearly linear pitching-moment characteristics and positive static longitudinal stability about a moment center at 55 percent of the length. With additional vertical surface in the form of a ventral fin, the configuration had directional stability and positive dihedral effect.

A 3 5 0

5. The complete configuration which showed favorable aerodynamic characteristics at low speeds was unsatisfactory at high subsonic speeds. A simulated "blow-away" fairing alleviated unfavorable lift and pitching-moment characteristics at Mach numbers of 0.85 and 0.90, but was detrimental at Mach numbers of 0.80 and less.

Ames Research Center
National Aeronautics and Space Administration
Moffett Field, Calif., Dec. 20, 1960

REFERENCES

1. Eggers, Alfred J., Jr., and Wong, Thomas J.: Re-entry and Recovery of Near-Earth Satellites, With Particular Attention to a Manned Vehicle. NASA MEMO 10-2-58A, 1958.

2. Savage, Howard F., and Tinling, Bruce E.: Subsonic Aerodynamic Characteristics of Several Blunt, Lifting, Atmospheric-Entry Shapes. NASA MFMO 12-24-58A, 1959.

3. Rakich, John V.: Supersonic Aerodynamic Performance and Static-Stability Characteristics of Two Blunt-Nosed, Modified 13° Half-Cone Configurations. NASA TM X-375, 1960.

4. Weil, Joseph, and Matranga, Gene J.: Review of Techniques Applicable to the Recovery of Lifting Hypervelocity Vehicles. NASA TM X-334, 1960.

5. Dennis, David H., and Edwards, George G.: The Aerodynamic Characteristics of Some Lifting Bodies. NASA TM X-376, 1960.

6. Herriot, John G.: Blockage Corrections for Three-Dimensional-Flow Closed-Throat Wind Tunnels, with Consideration of the Effect of Compressibility. NACA Rep. 995, 1950. (Supersedes NACA RM A7B28).

7. Bray, Richard S., Drinkwater, Fred J. III, and White, Maurice D.: A Flight Study of a Power-Off Landing Technique Applicable to Re-entry Vehicles. NASA TN D-323, 1960.

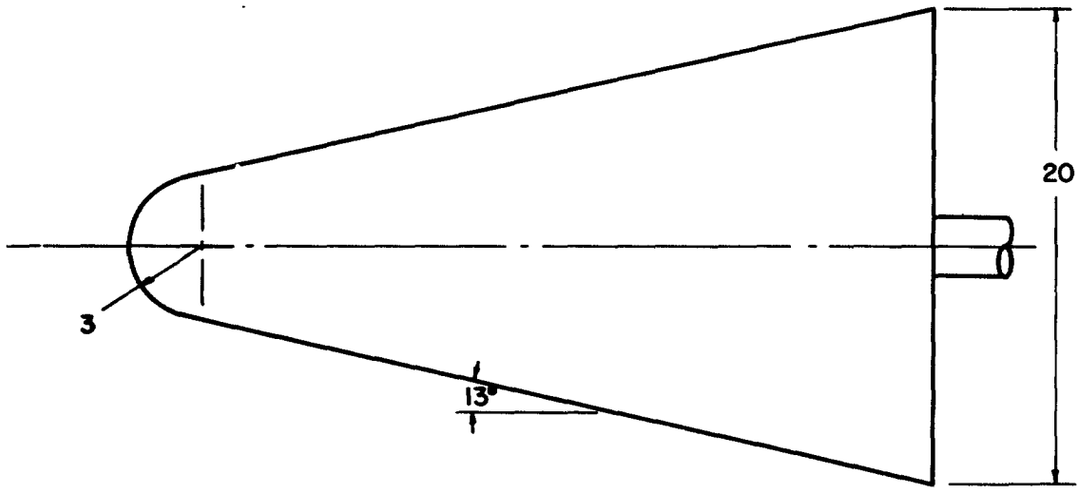

Plan area 2.82 sq. ft.
Base area 1.33 sq. ft.

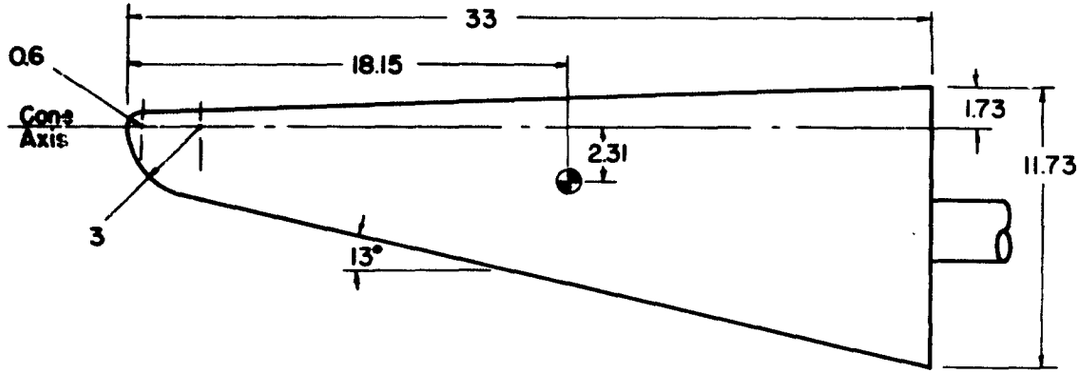

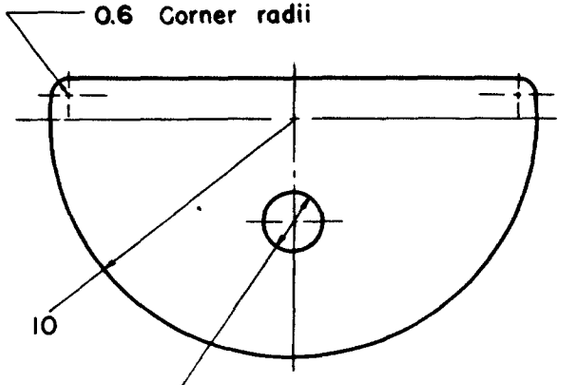

All dimension in inches

Figure 1.- The geometry of body 1.

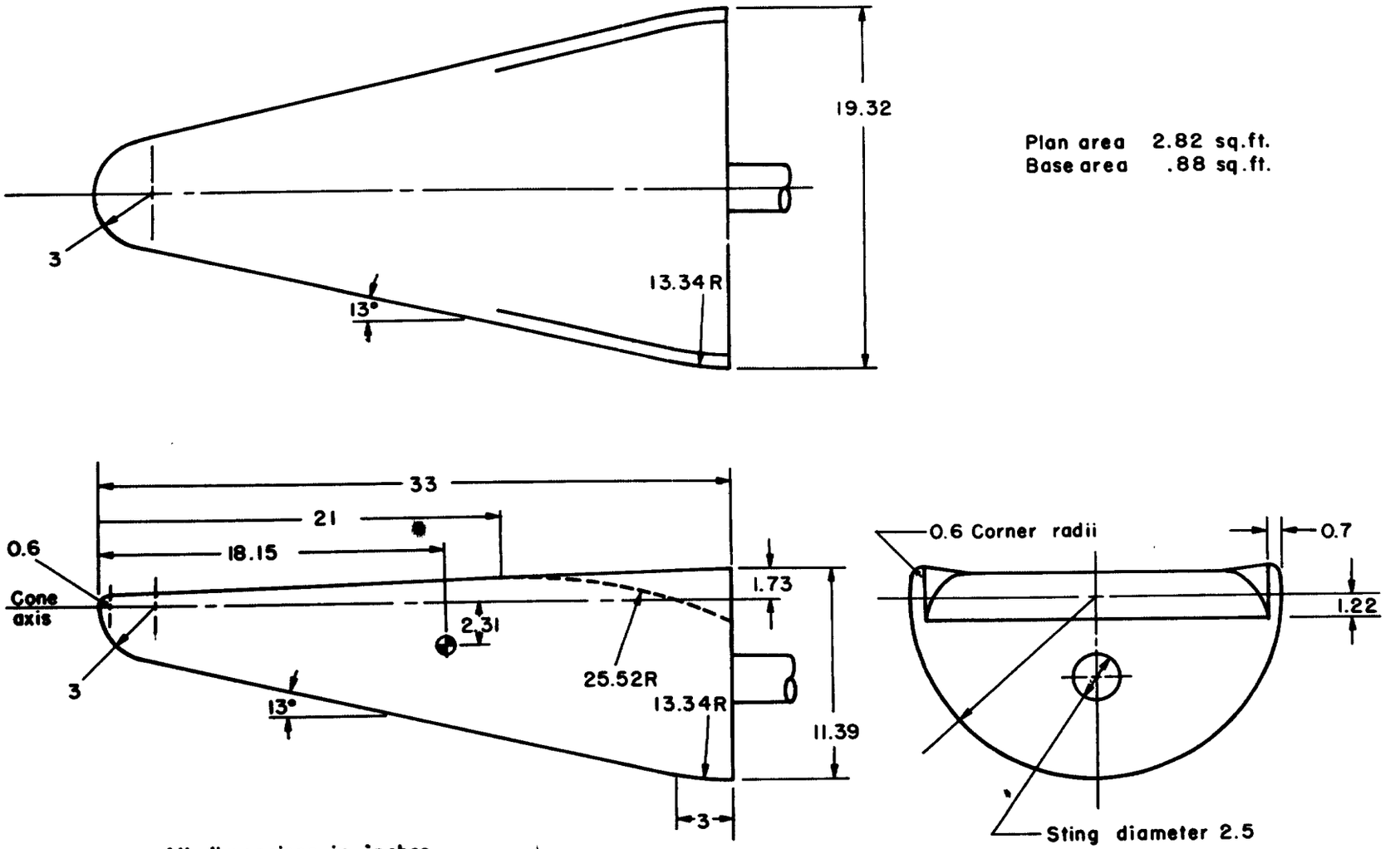

Figure 2.- The geometry of body 2.

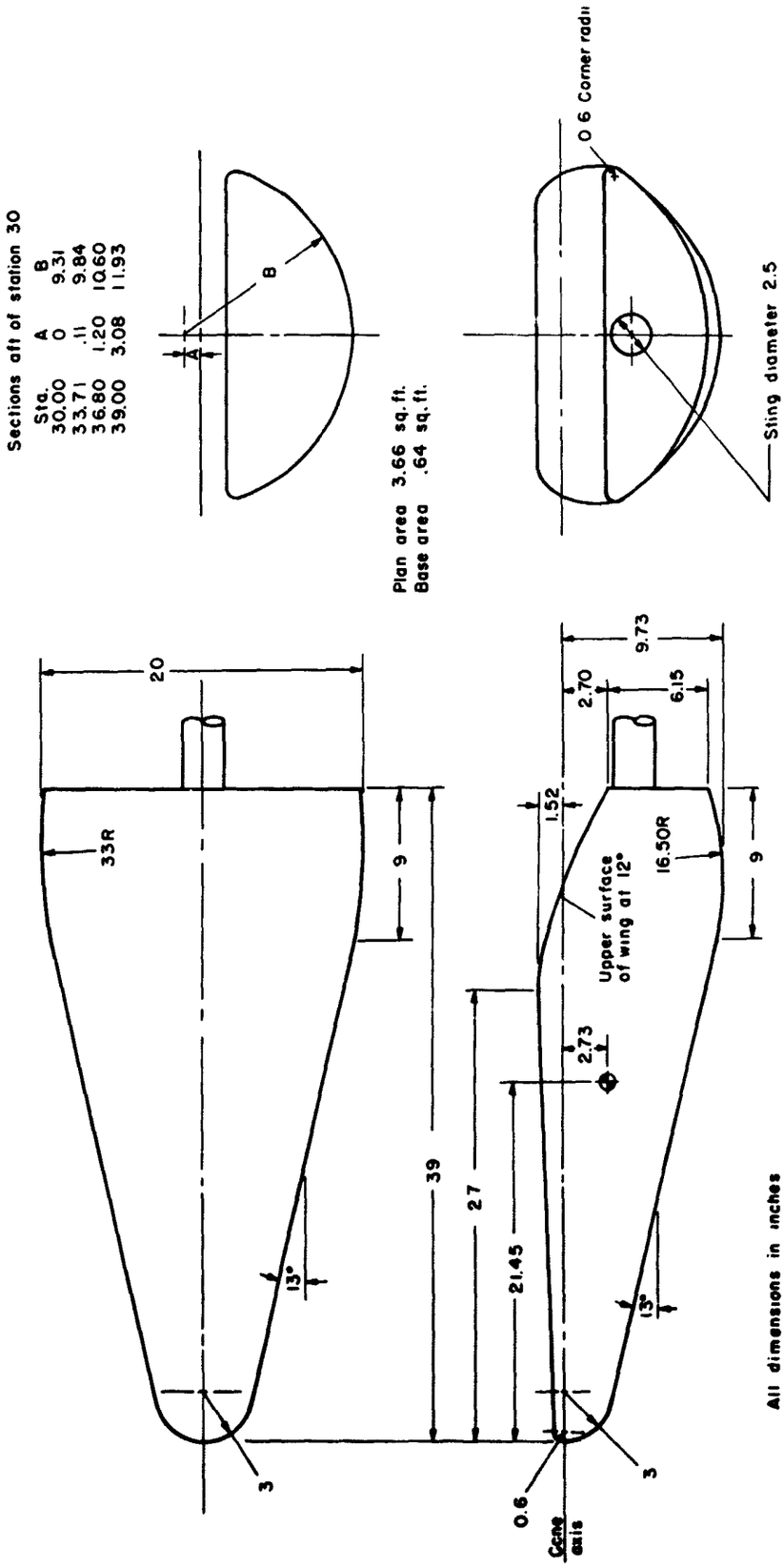

Figure 3.- The geometry of body 3.

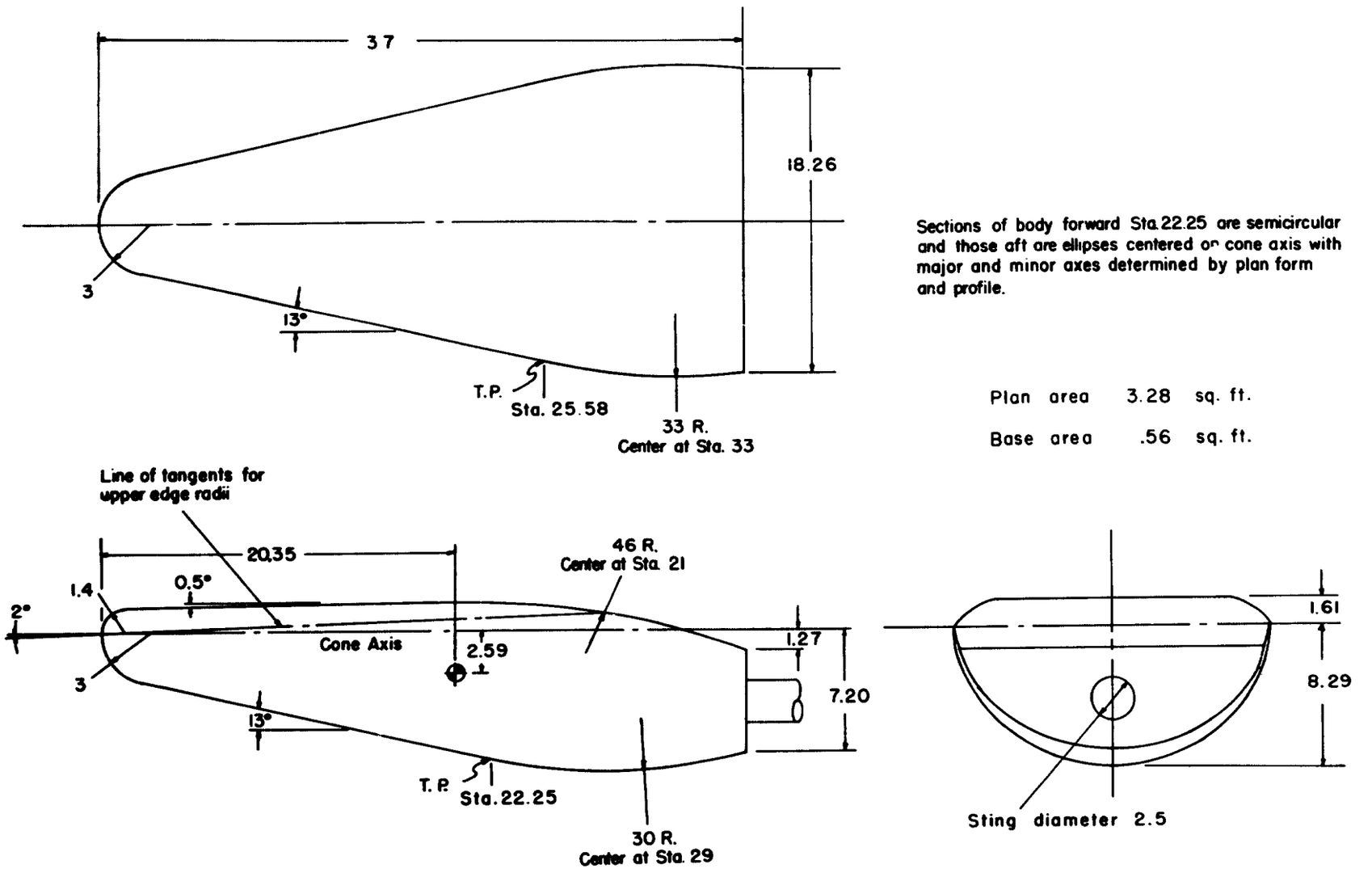

Sections of body forward Sta 22.25 are semicircular and those aft are ellipses centered on cone axis with major and minor axes determined by plan form and profile.

Plan area	3.28	sq. ft.
Base area	.56	sq. ft.

Figure 4.- The geometry of body 4.

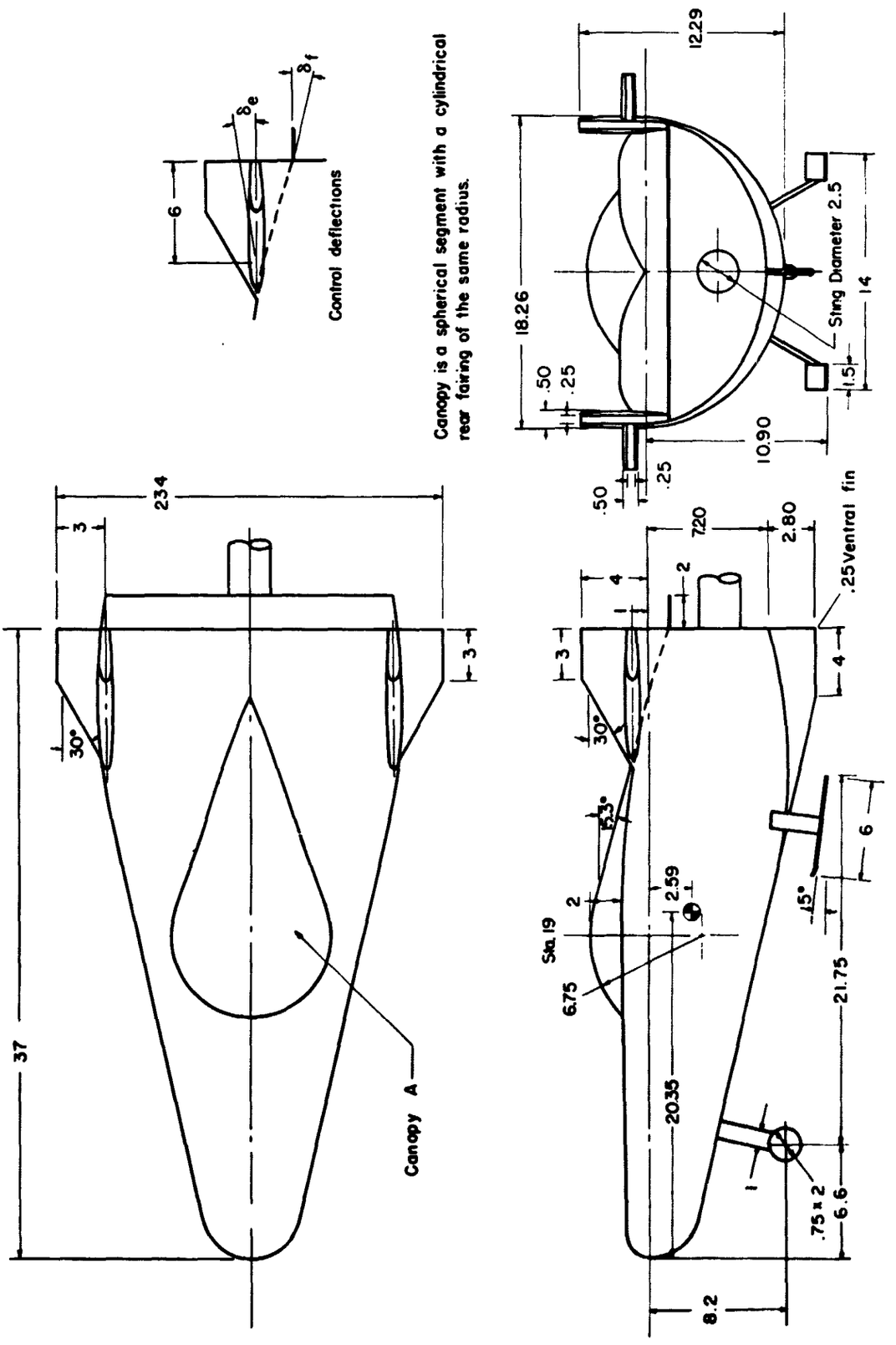

Figure 5.- Body 4 with the vertical surfaces, trailing-edge flap, elevons, canopy A, landing gear, and ventral fin.

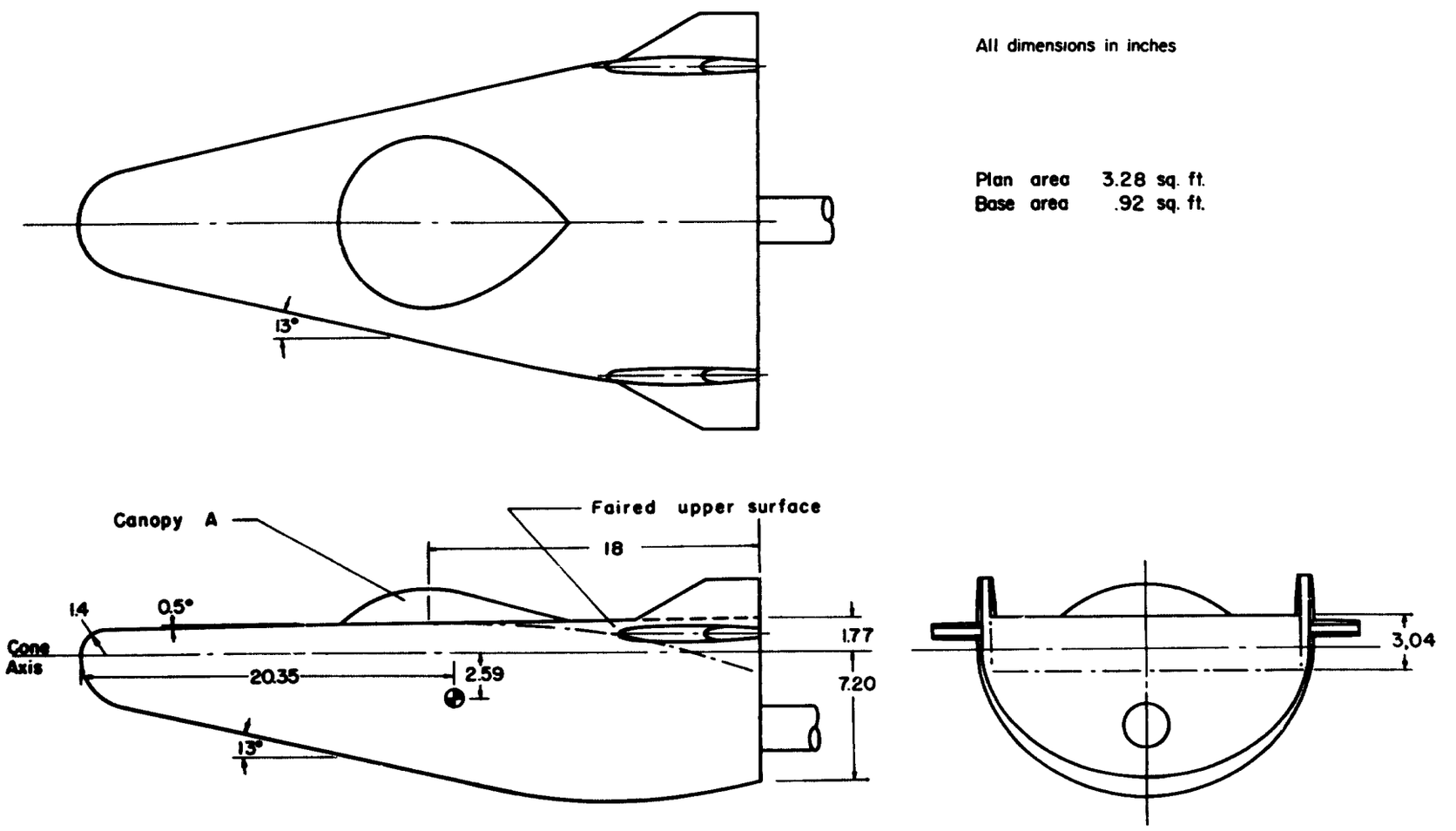

Figure 6.- Body 4 with the upper surface fairing.

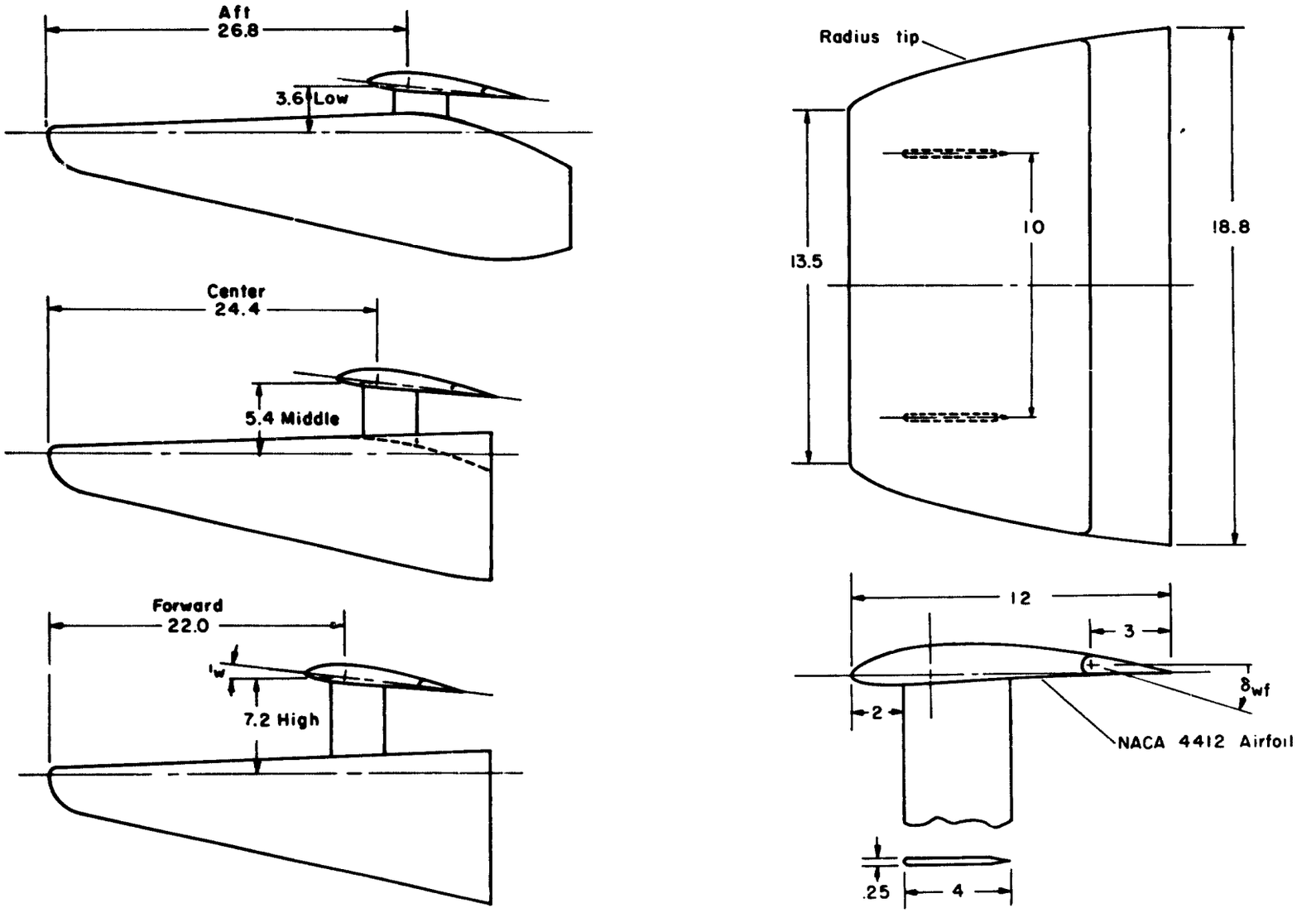

Figure 7.- The geometry of the auxiliary wing and its positions with respect to bodies , 2, and 3.

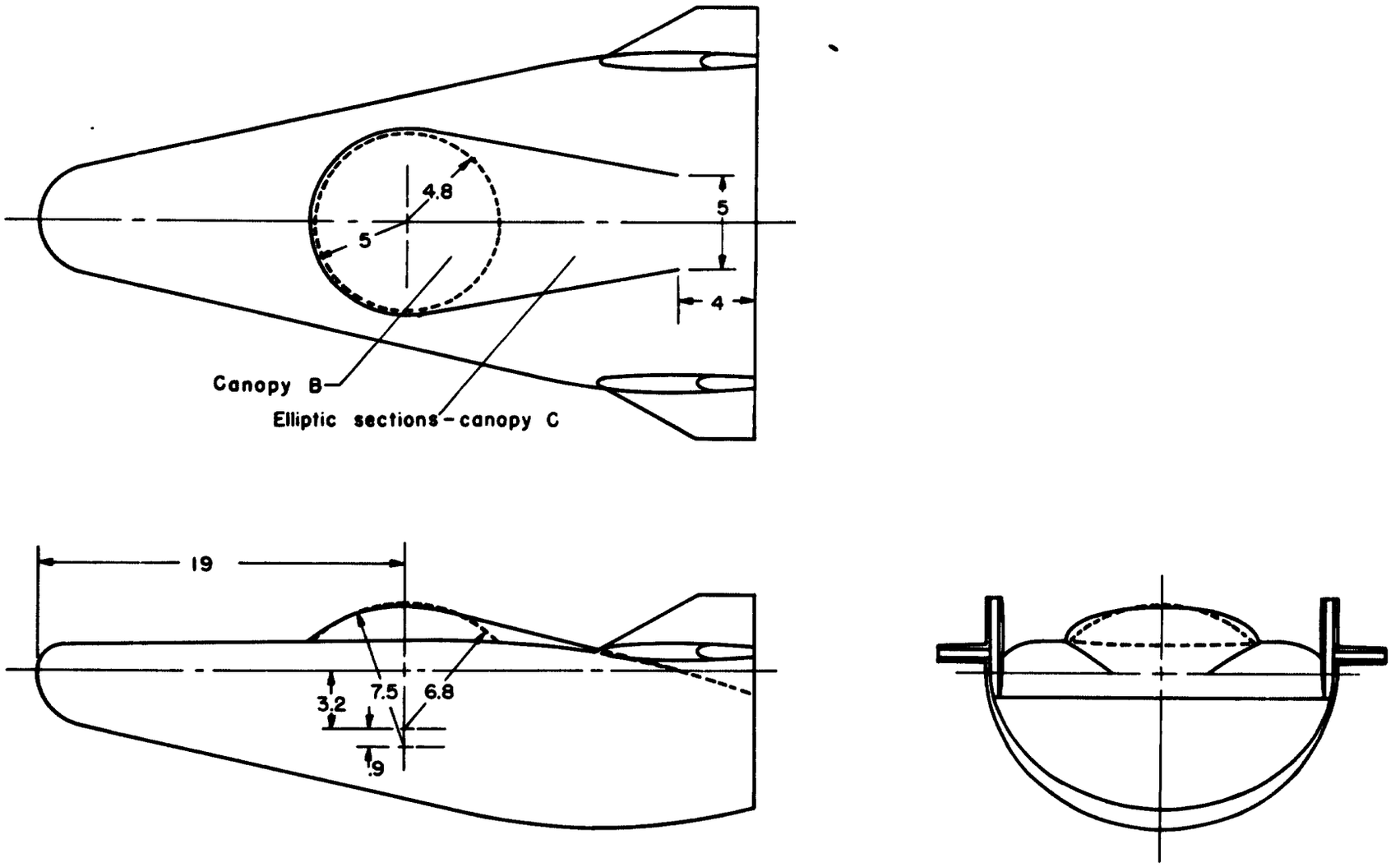

(a) Canopies B and C.

Figure 8.- The geometry of canopies B, C, and D.

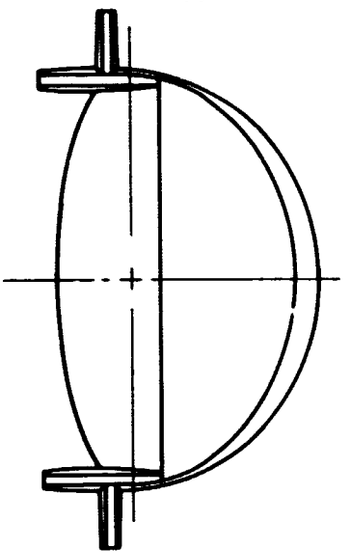

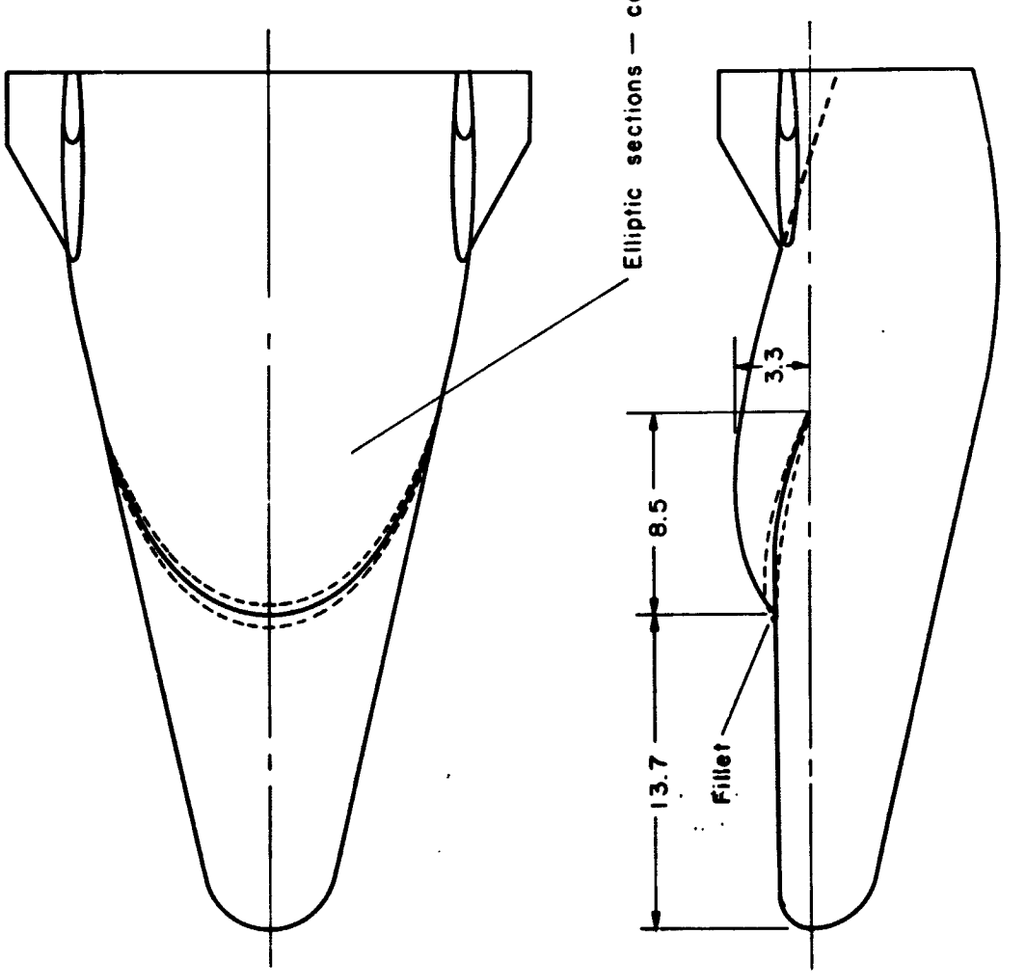

(b) Canopy D.

Figure 8.- Concluded.

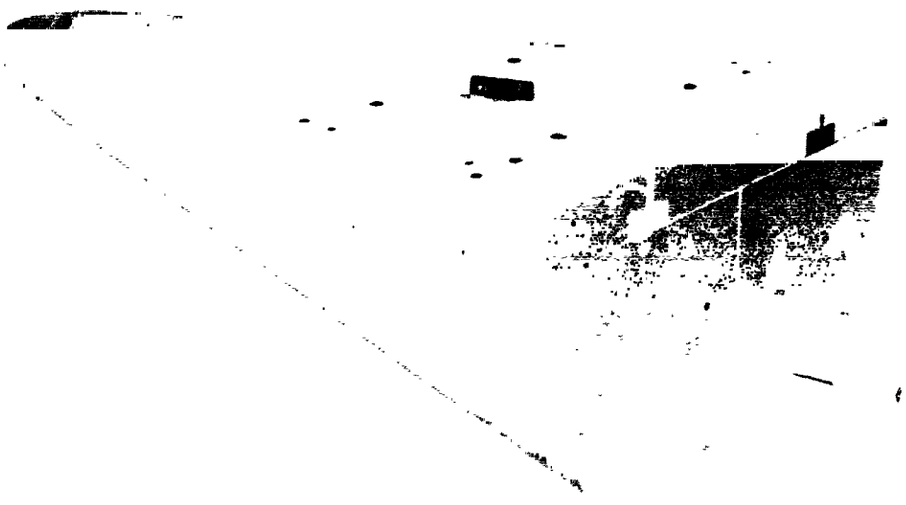

(a) Body 1. A-25128

(b) Body 2. A-25126

Figure 9.- Photographs of the models.

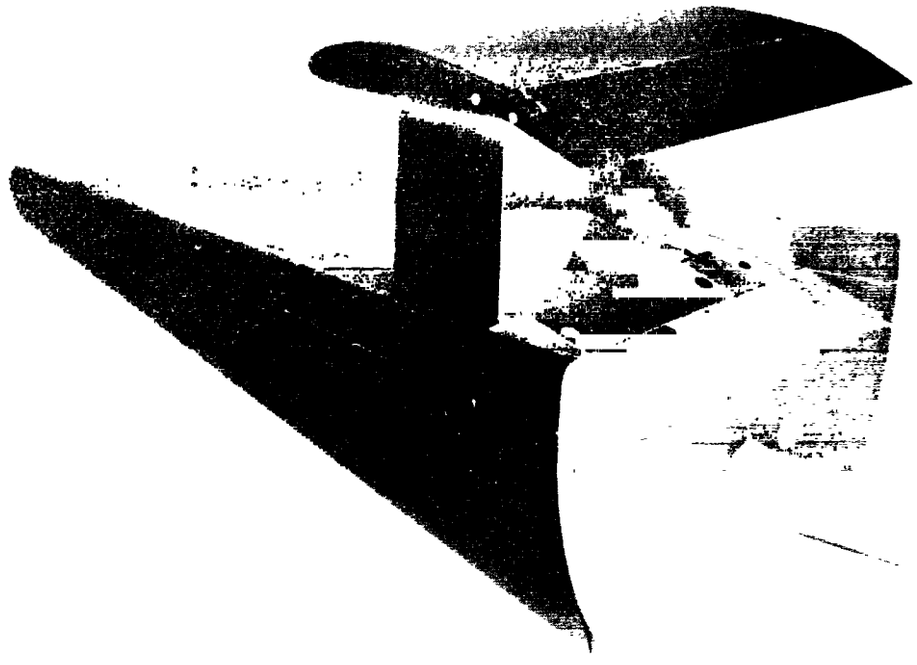

(c) Body 2 with the auxiliary wing. A-25127

(d) Body 3. A-25129

Figure 9.- Continued.

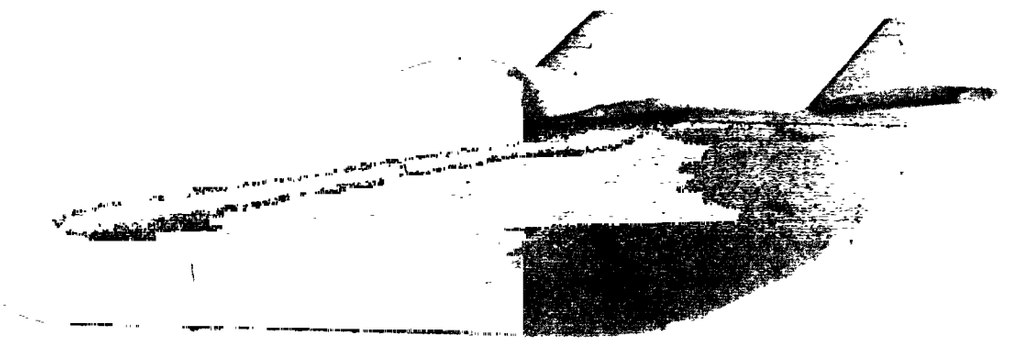

A-25964

(e) Body 4 with canopy A, vertical surfaces, elevons, and landing gear.

Figure 9.- Concluded.

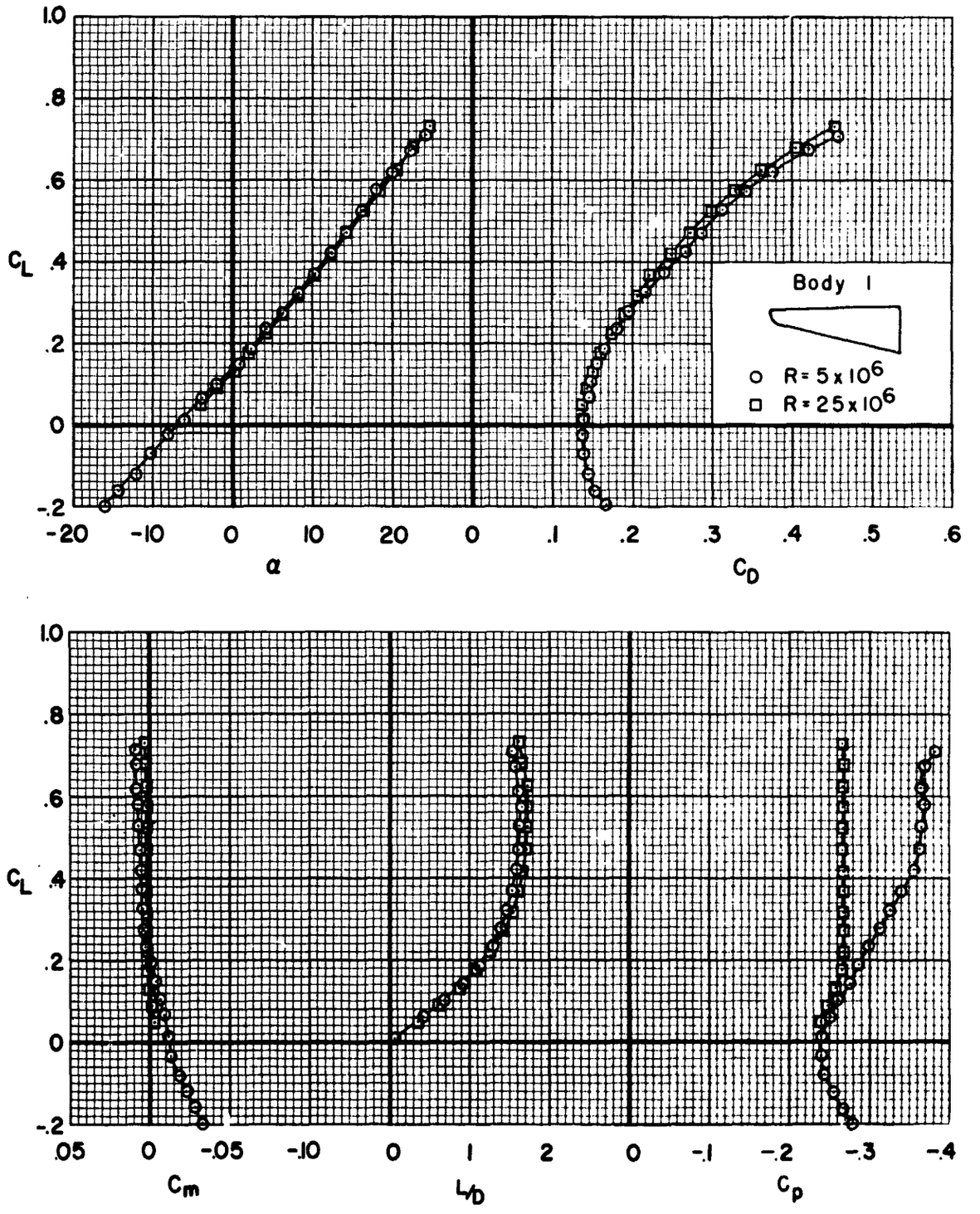

Figure 10.- The static longitudinal aerodynamic characteristics of body 1 for two Reynolds numbers; M = 0.25.

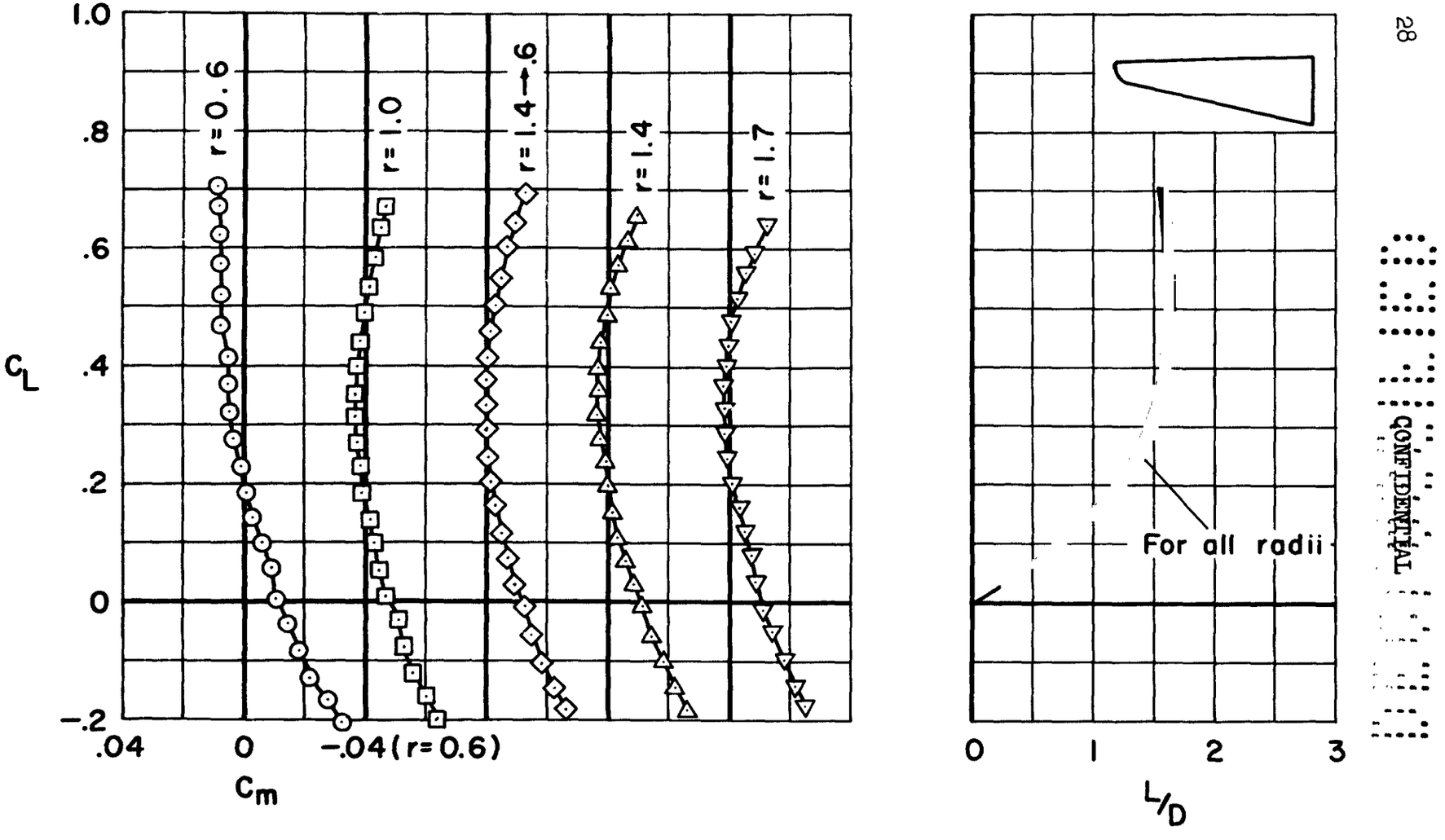

Figure 11.- The effects of variations in the leading-edge radius on the stability and performance of body 1; M = 0.25, R = 5×10^6.

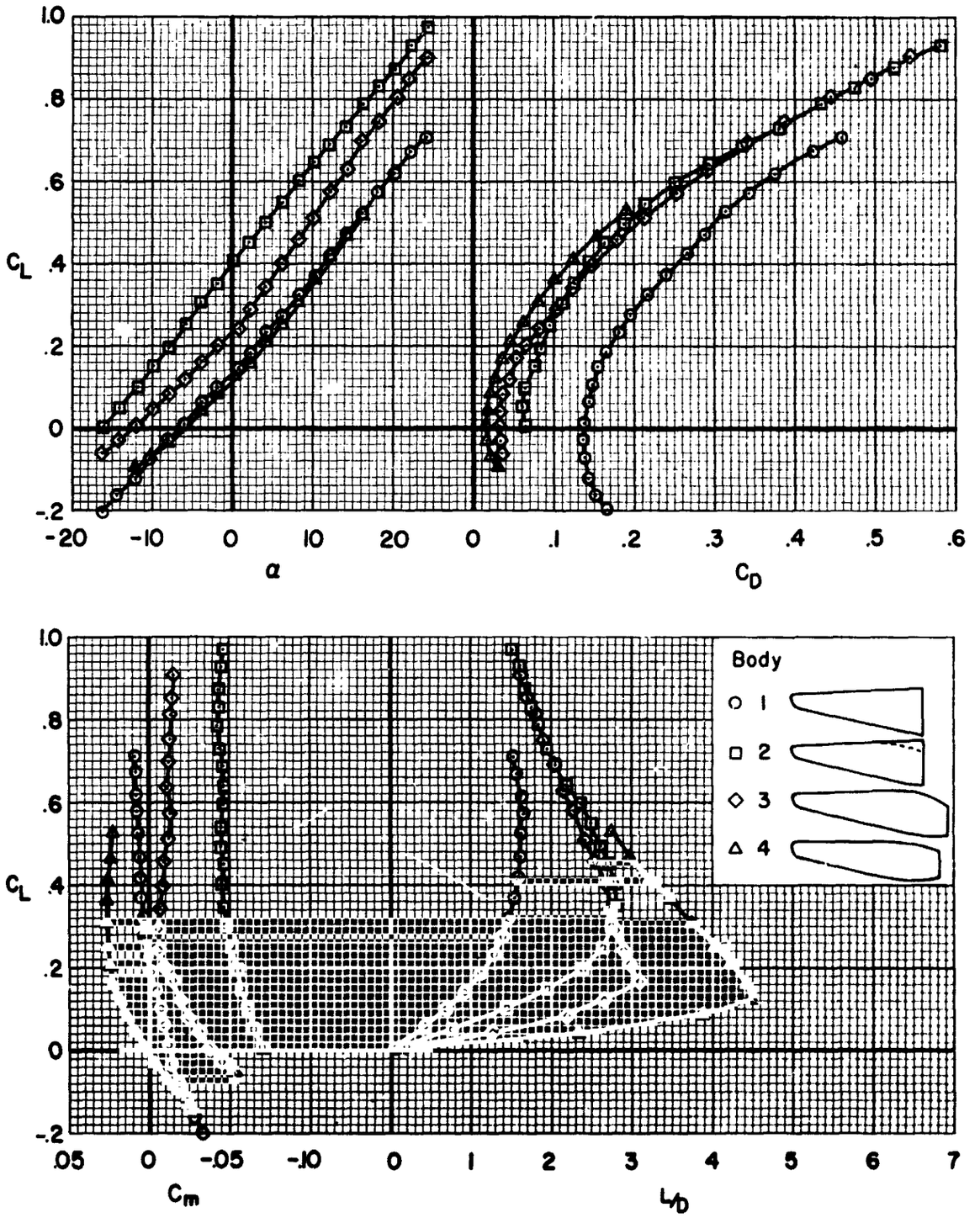

Figure 12.- The longitudinal characteristics of bodies 1, 2, 3, and 4; M = 0.25, R = 5×10^6.

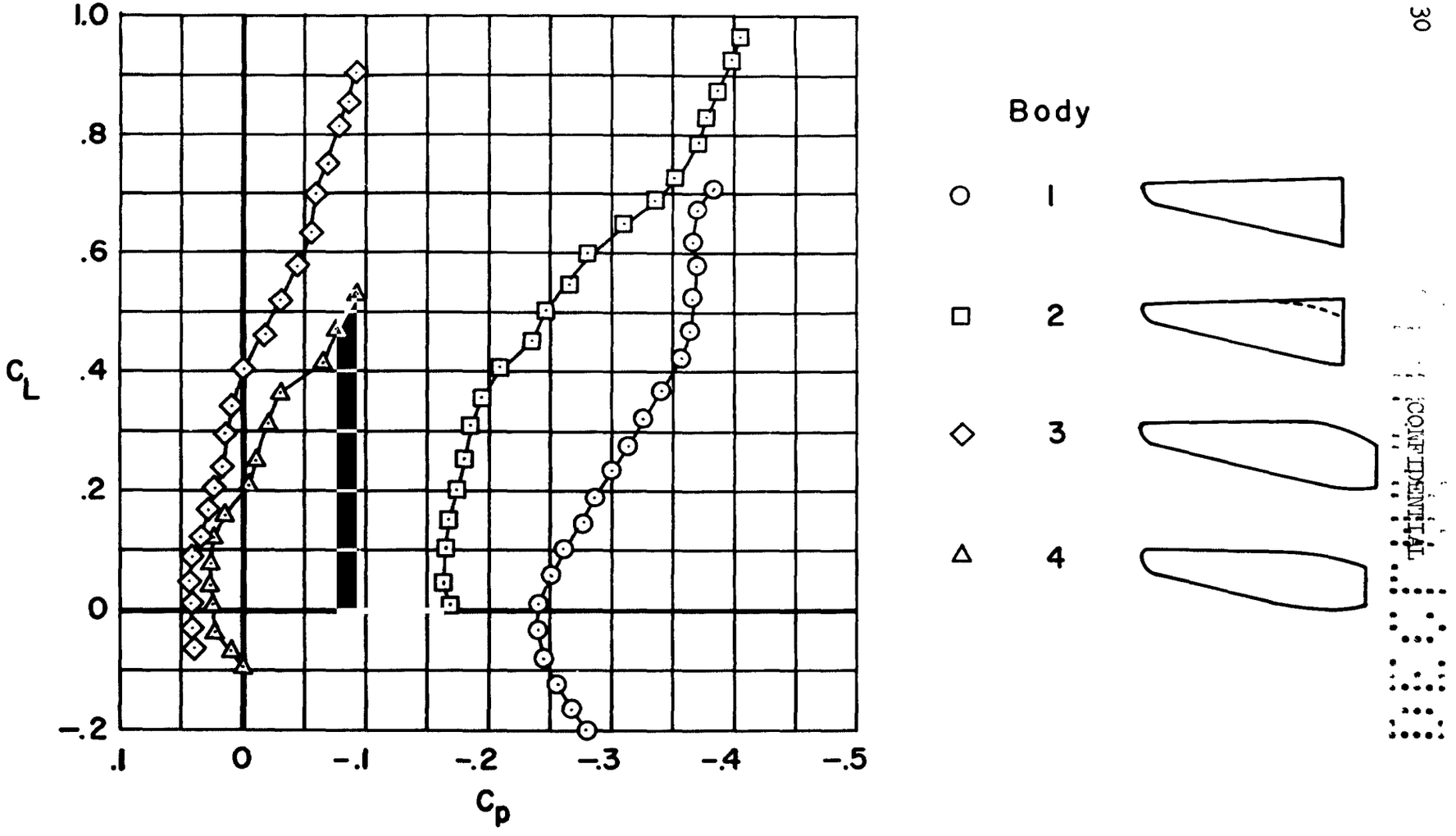

Figure 13.- The base-pressure coefficients for bodies 1, 2, 3, and 4; M = 0.25, R = 5×10^6.

(a) $\alpha = 0^{\circ}$

(b) $\alpha = 8^{\circ}$

(c) $\alpha = 16^{\circ}$

(d) $\alpha = 24^{\circ}$

Figure 14.- The vortex formation above the surface of body 3, as shown by a tuft grid; $M = 0.25$. $R = 5 \times 10^6$.

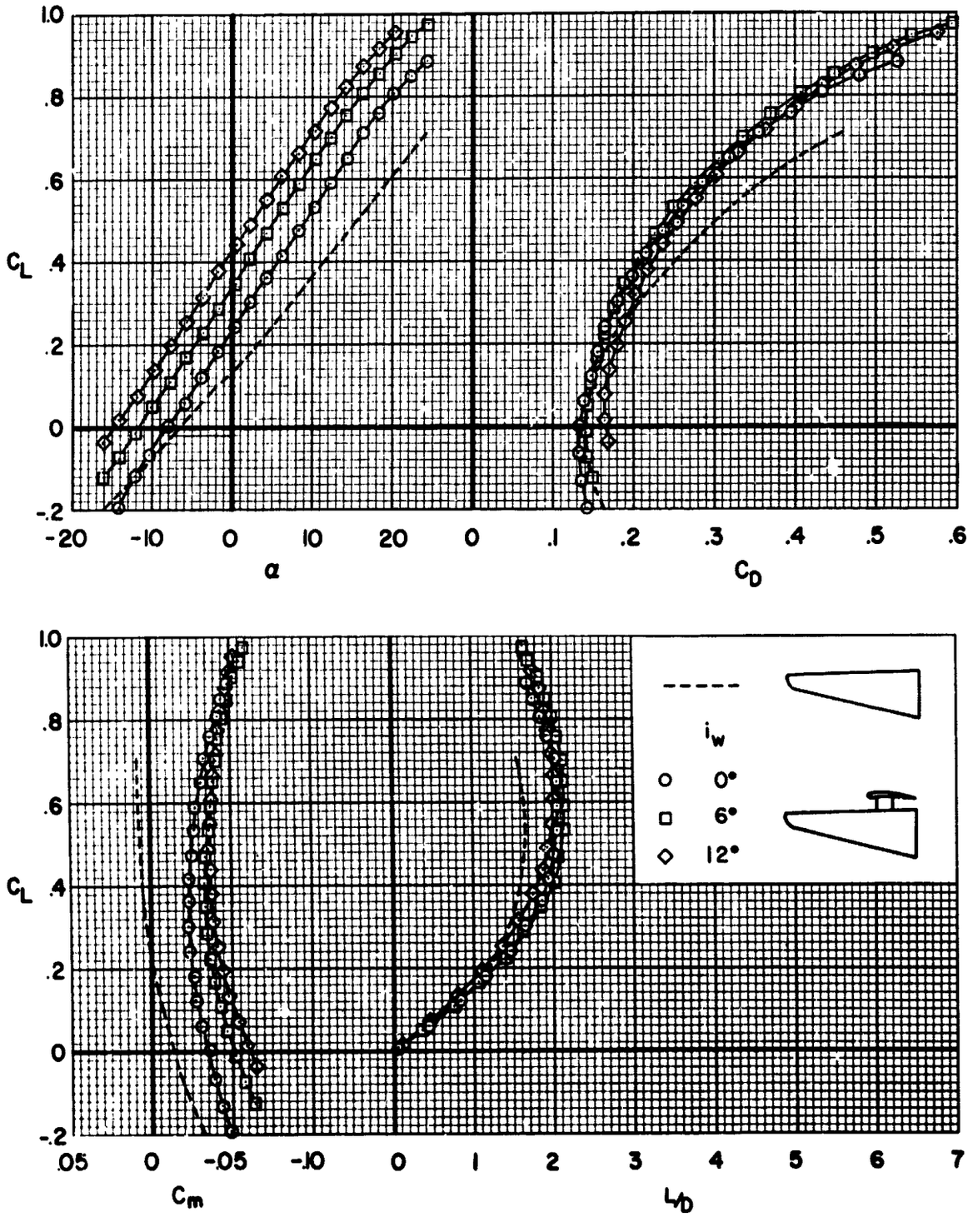

Figure 15.- The effects of the incidence of the auxiliary wing (in the high forward position) on the longitudinal characteristics of body 1; M = 0.25, R = 5×10^6, $\delta_{wf} = 0^\circ$.

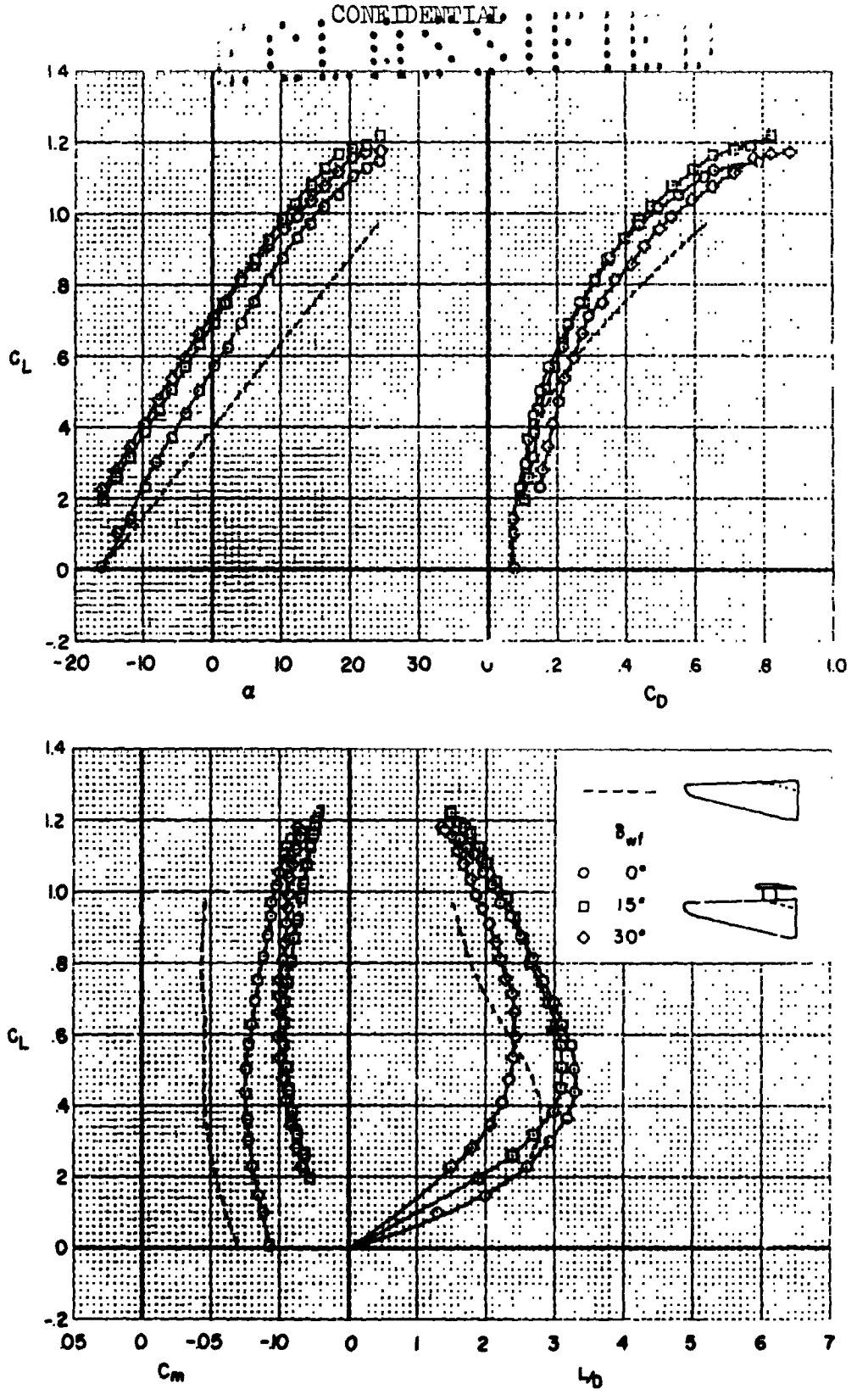

Figure 16.- The effects of flap deflection of the auxiliary wing (in the high center position) on the longitudinal characteristics of body 2; $M = 0.25$, $R \approx 5 \times 10^6$, $i_w = 12^\circ$.

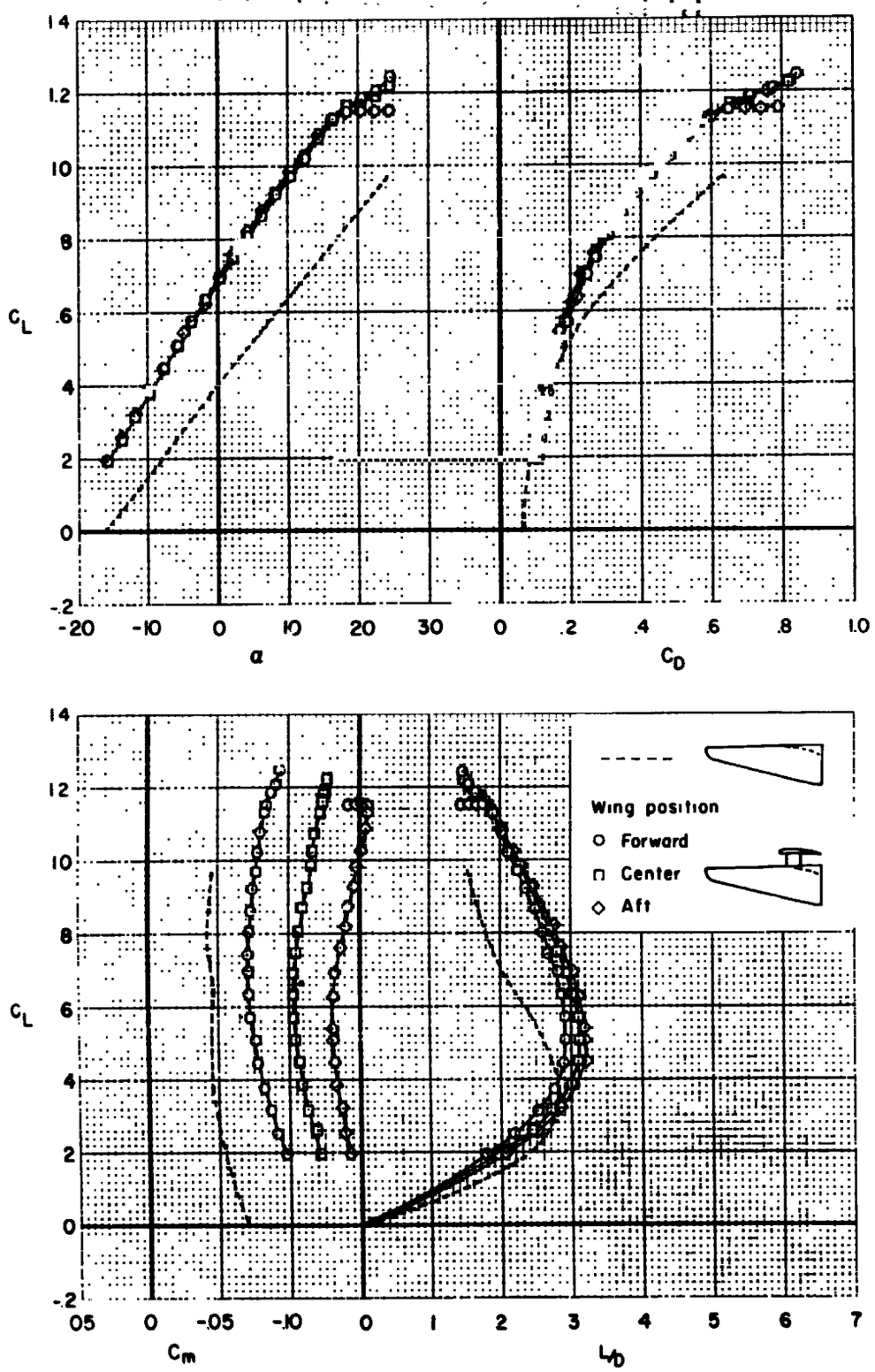

Figure 17.- The effects of the longitudinal location of the auxiliary wing (in the high position) on the longitudinal characteristics of body 2; M = 0.25, R = 5×10^6, $i_w = 12^\circ$, $\delta_{wf} = 15^\circ$.

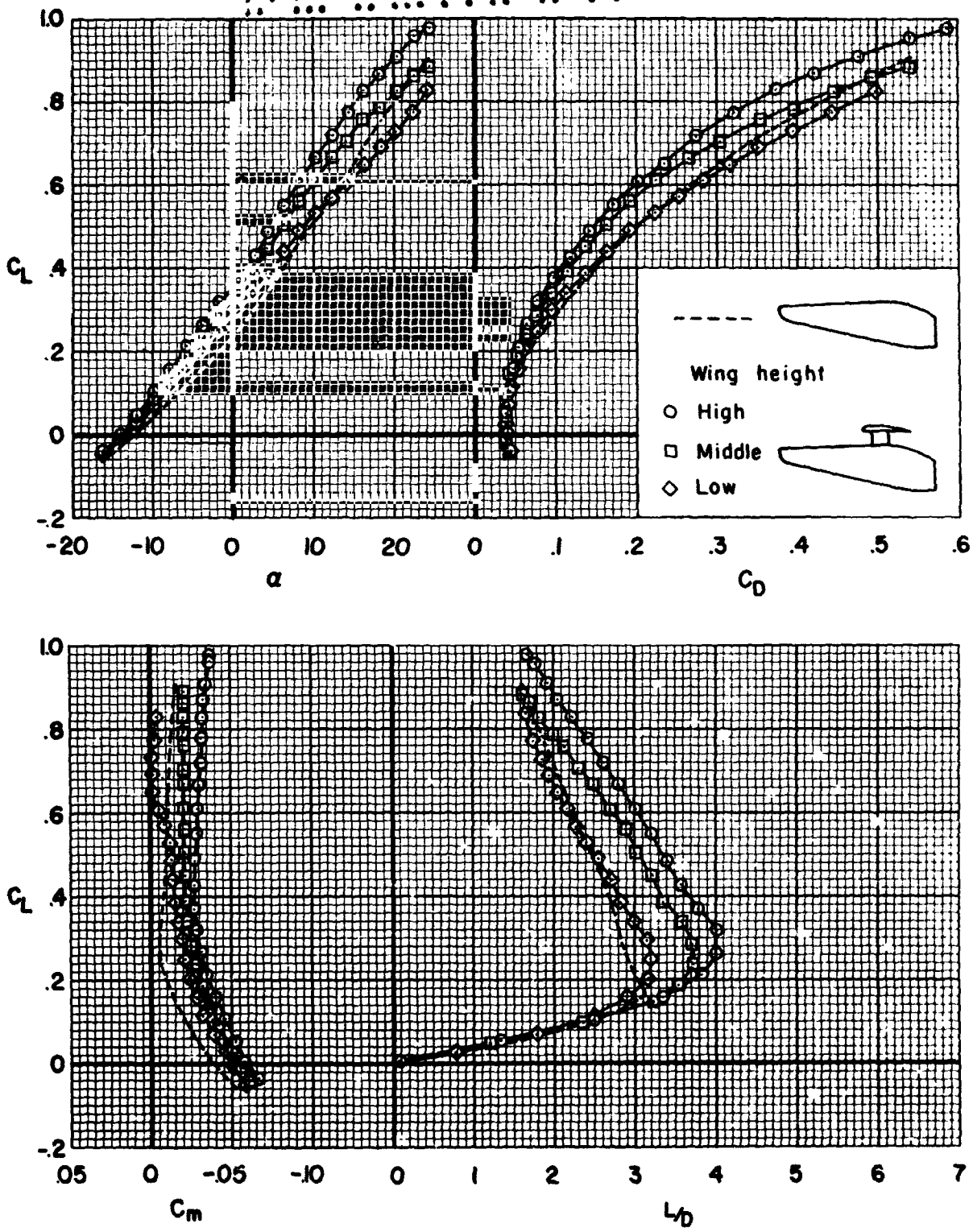

Figure 18.- The effects of the height of the auxiliary wing (in the aft position) on the longitudinal characteristics of body 3; M = 0.25, R = 5x10^6, $i_w = 12^\circ$, $\delta_{wf} = 0^\circ$.

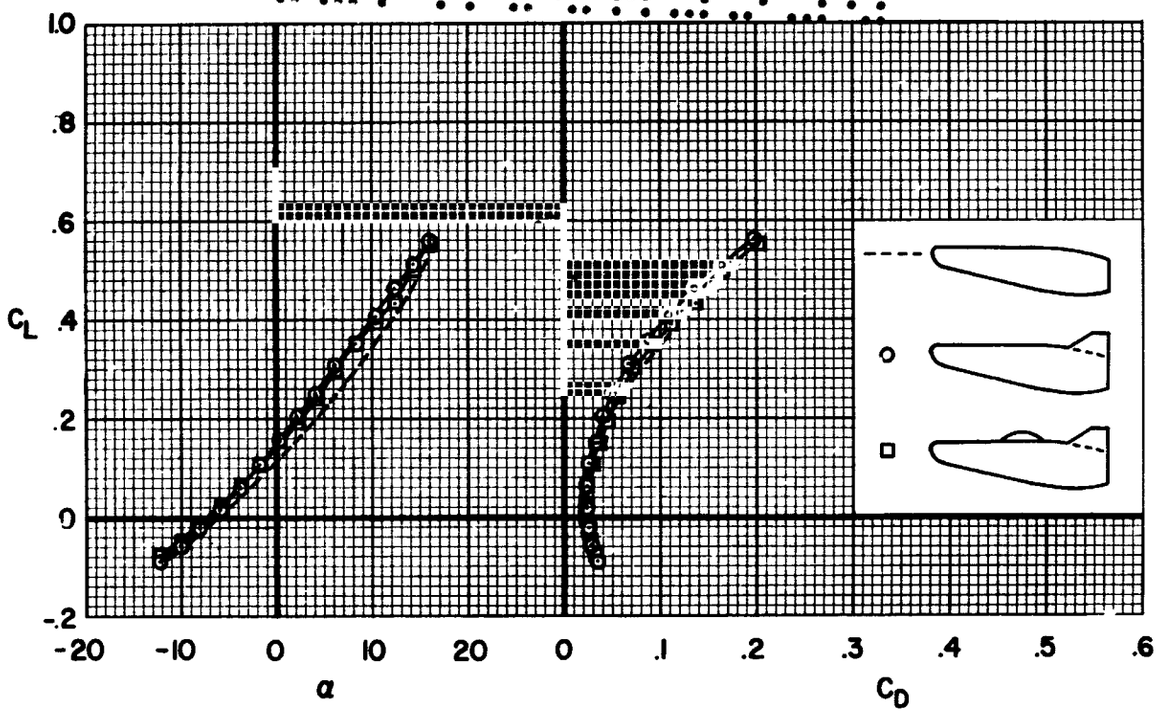

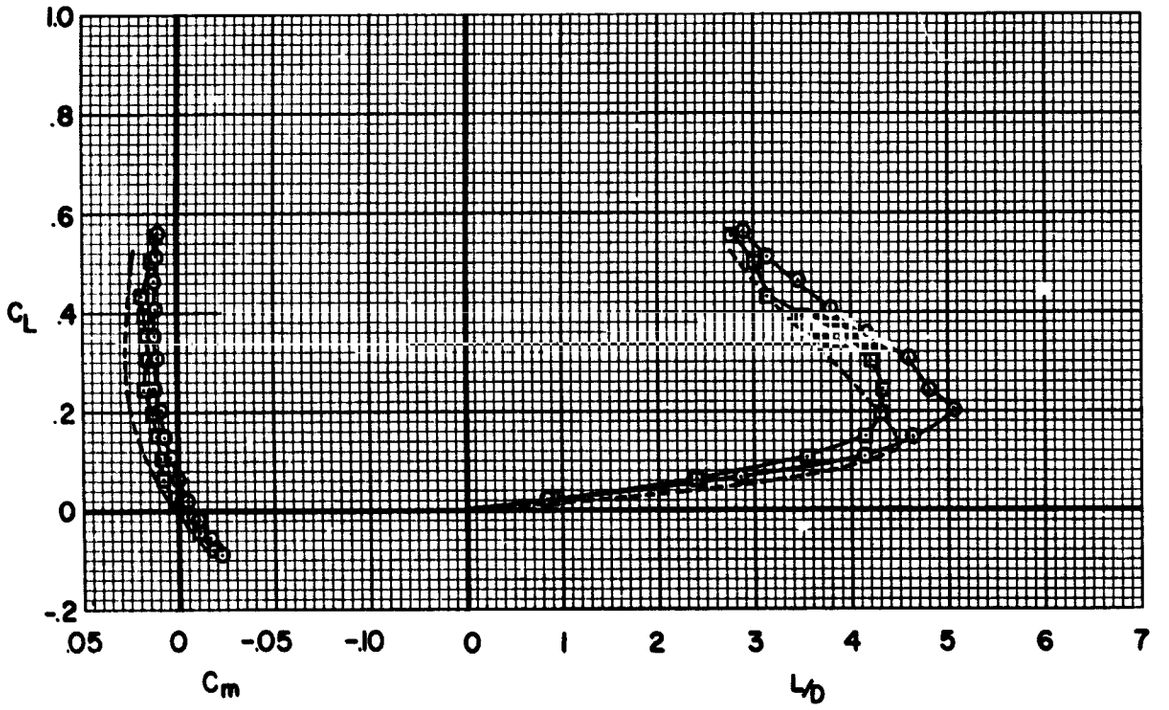

Figure 19.- The effects of the vertical surfaces and canopy B on the longitudinal characteristics of body 4; M = 0.25, R = 5×10^6.

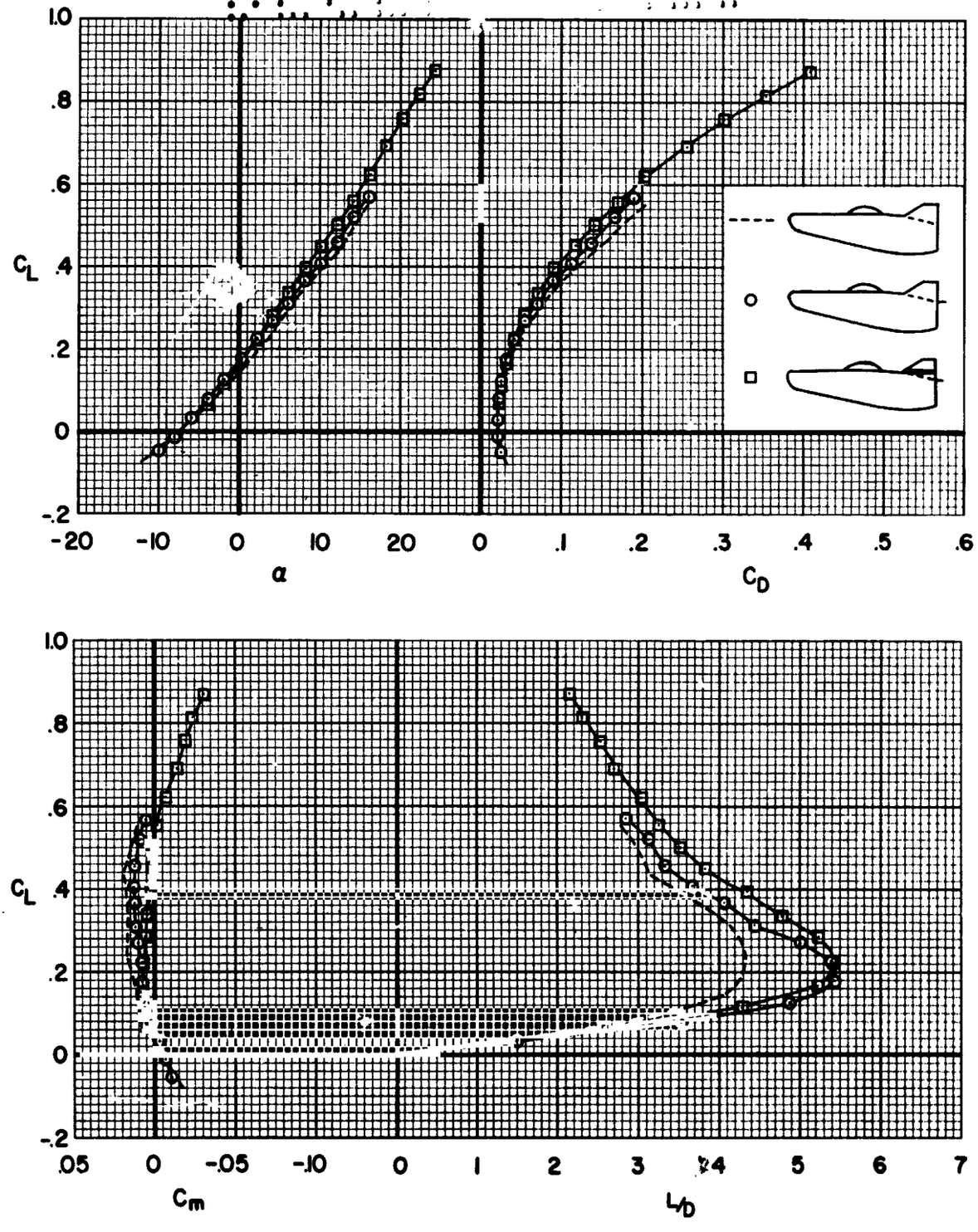

Figure 20.- The effects of the trailing-edge flap and elevon on the longitudinal characteristics of body 4 with canopy B; M = 0.25, $R = 5 \times 10^6$, $\delta_f = -5^\circ$, $\delta_e = 0^\circ$.

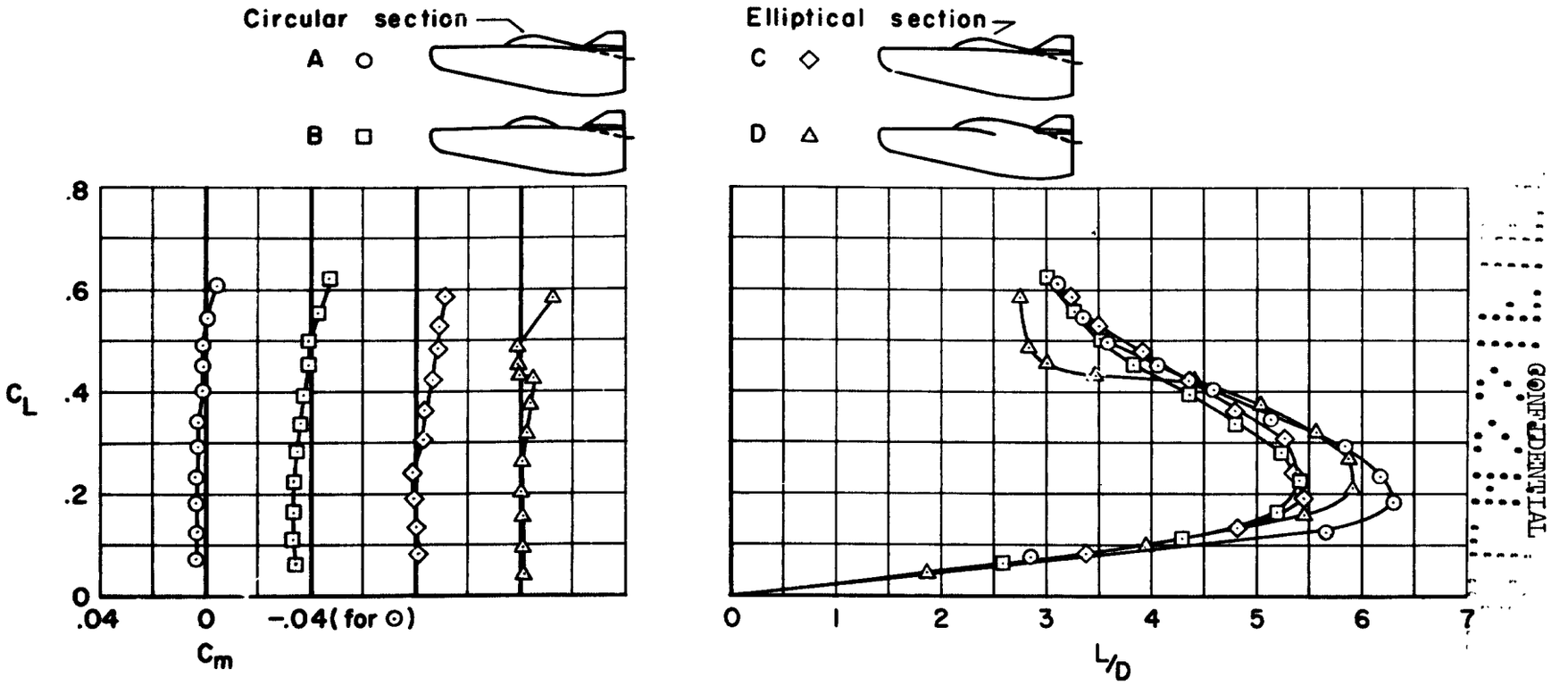

Figure 21.- The effects of canopy variations on the stability and performance of body 4 with vertical surfaces, elevons, and trailing-edge flap; M = 0.25, R = 5×10^6, $\delta_f = -5^\circ$, $\delta_e = 0^\circ$.

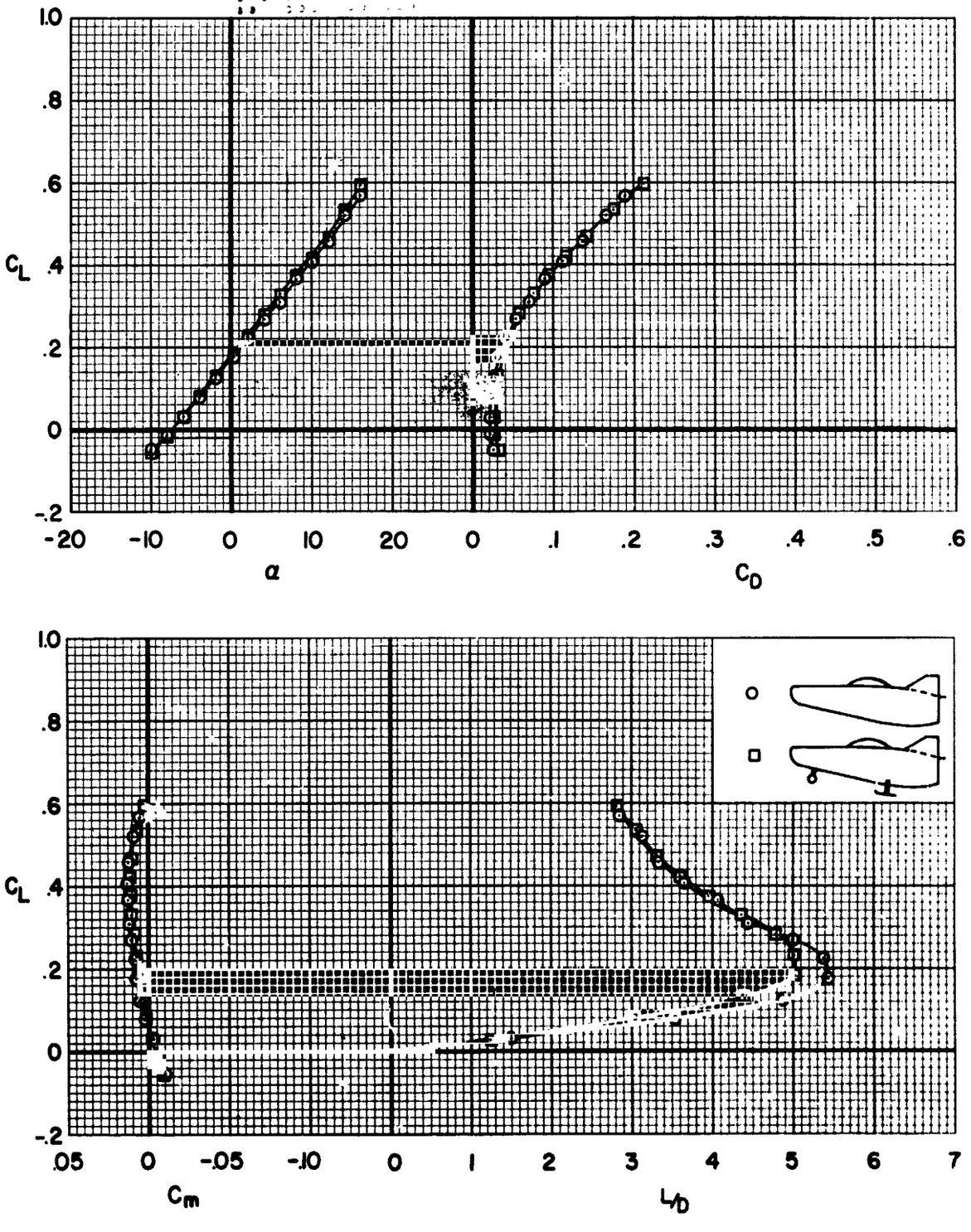

Figure 22.- The effects of the landing gear on the longitudinal characteristics of body 4 with canopy B, vertical surfaces, and trailing-edge flap (elevons off); M = 0.25, R = 5×10^6, $\delta_e = -5^\circ$.

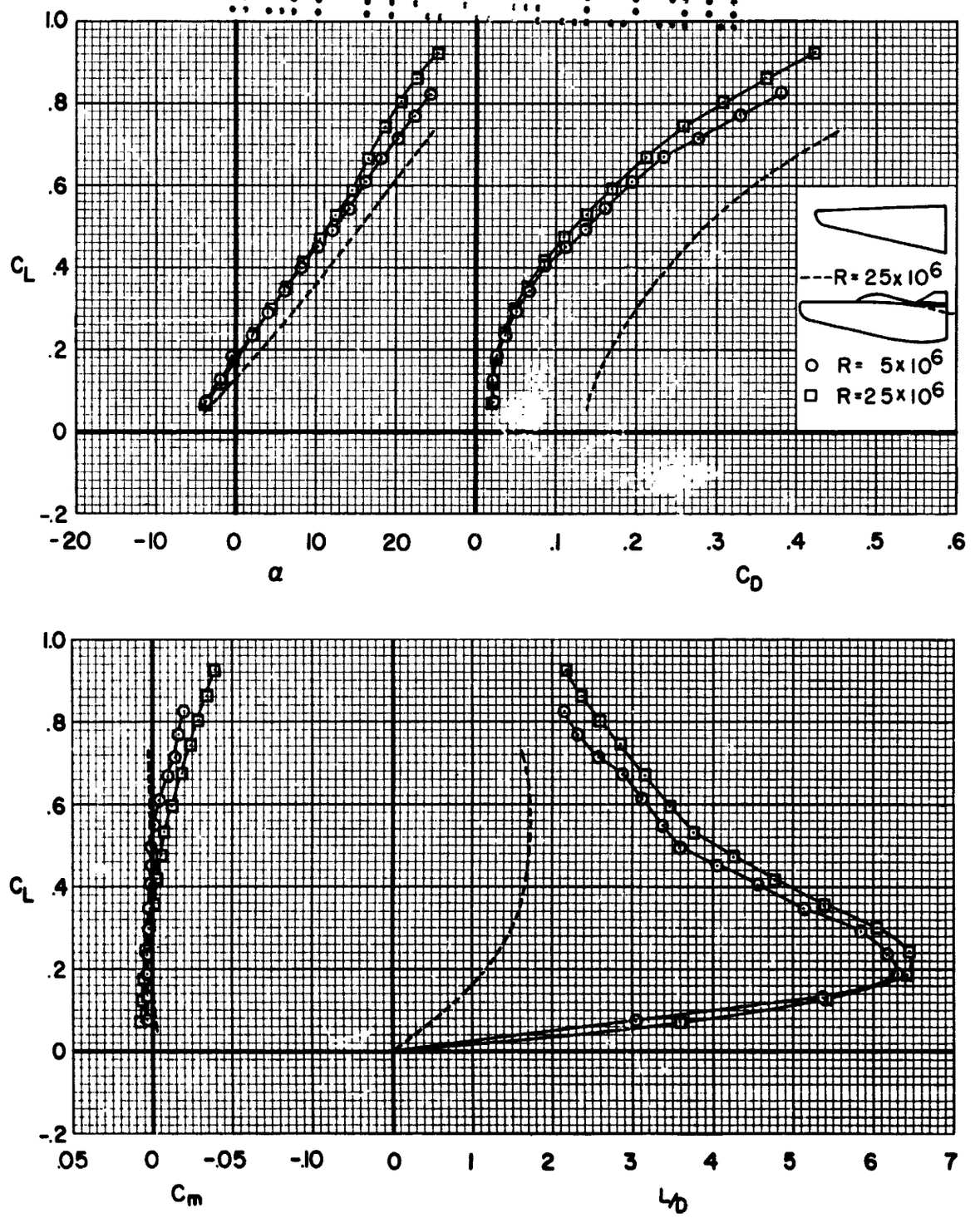

Figure 23.- The effects of Reynolds number on the longitudinal characteristics of the complete configuration with body 4 and canopy A; M = 0.25, $\delta_f = -5^\circ$, $\delta_e = 0^\circ$.

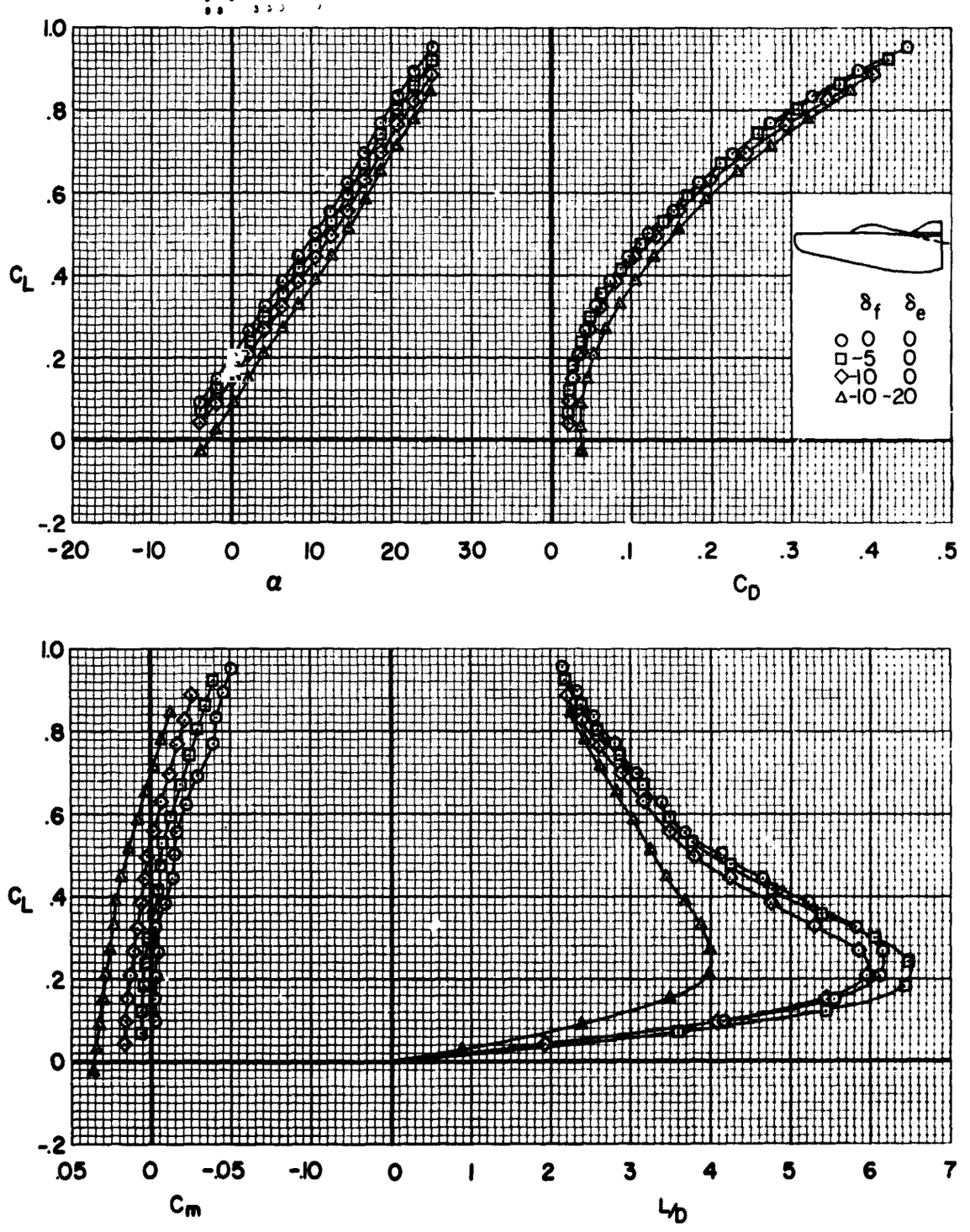

Figure 24.- The effects of elevon and trailing-edge flap deflection on the longitudinal characteristics of the complete configuration with body 4 and canopy A; M = 0.25, R = 25x10^6.

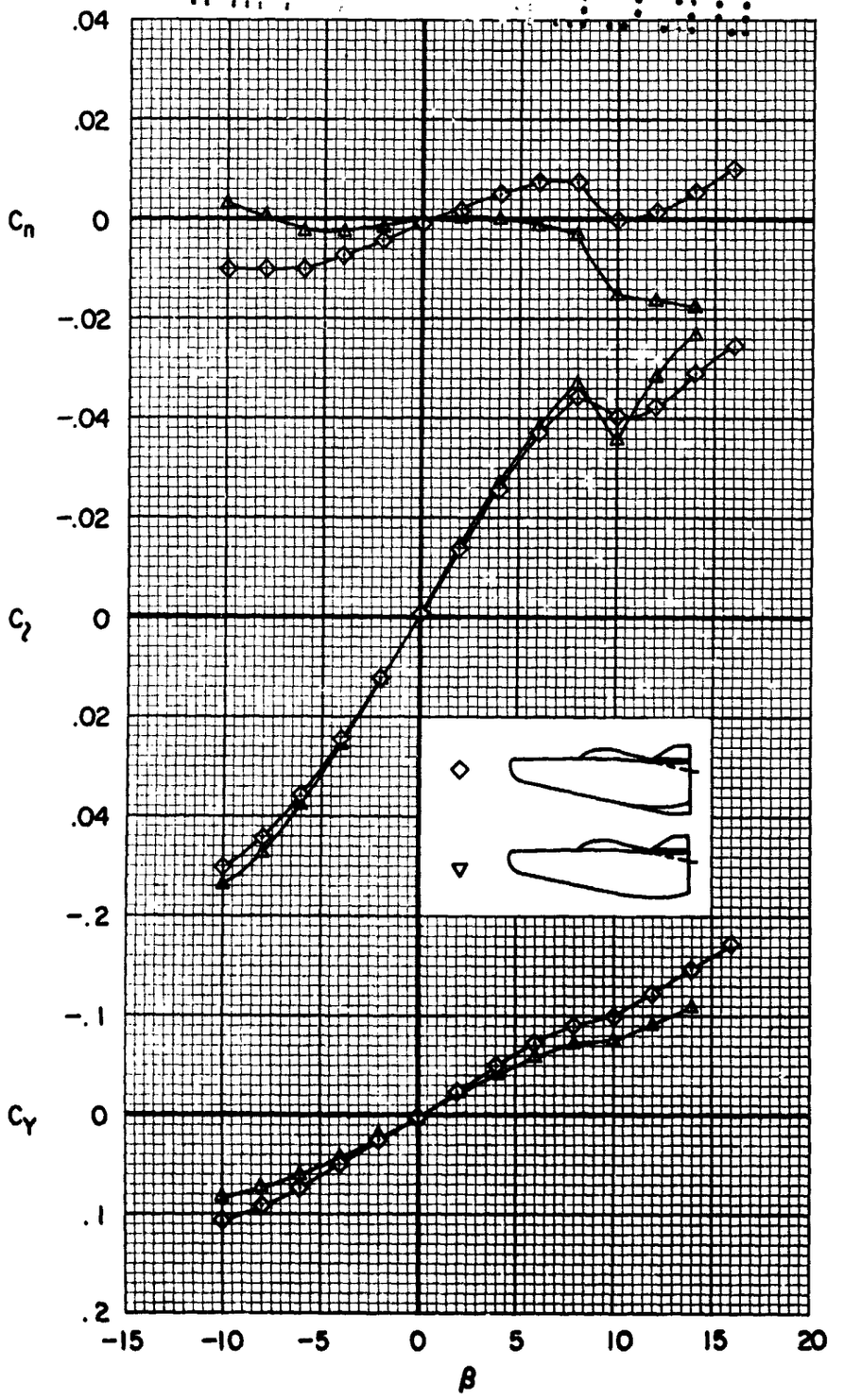

Figure 25.- The effects of the ventral fin on the lateral and directional characteristics of the complete configuration at 6° angle of attack; M = 0.25, R = 25x10^6, δ_e = 0°, δ_f = -5°.

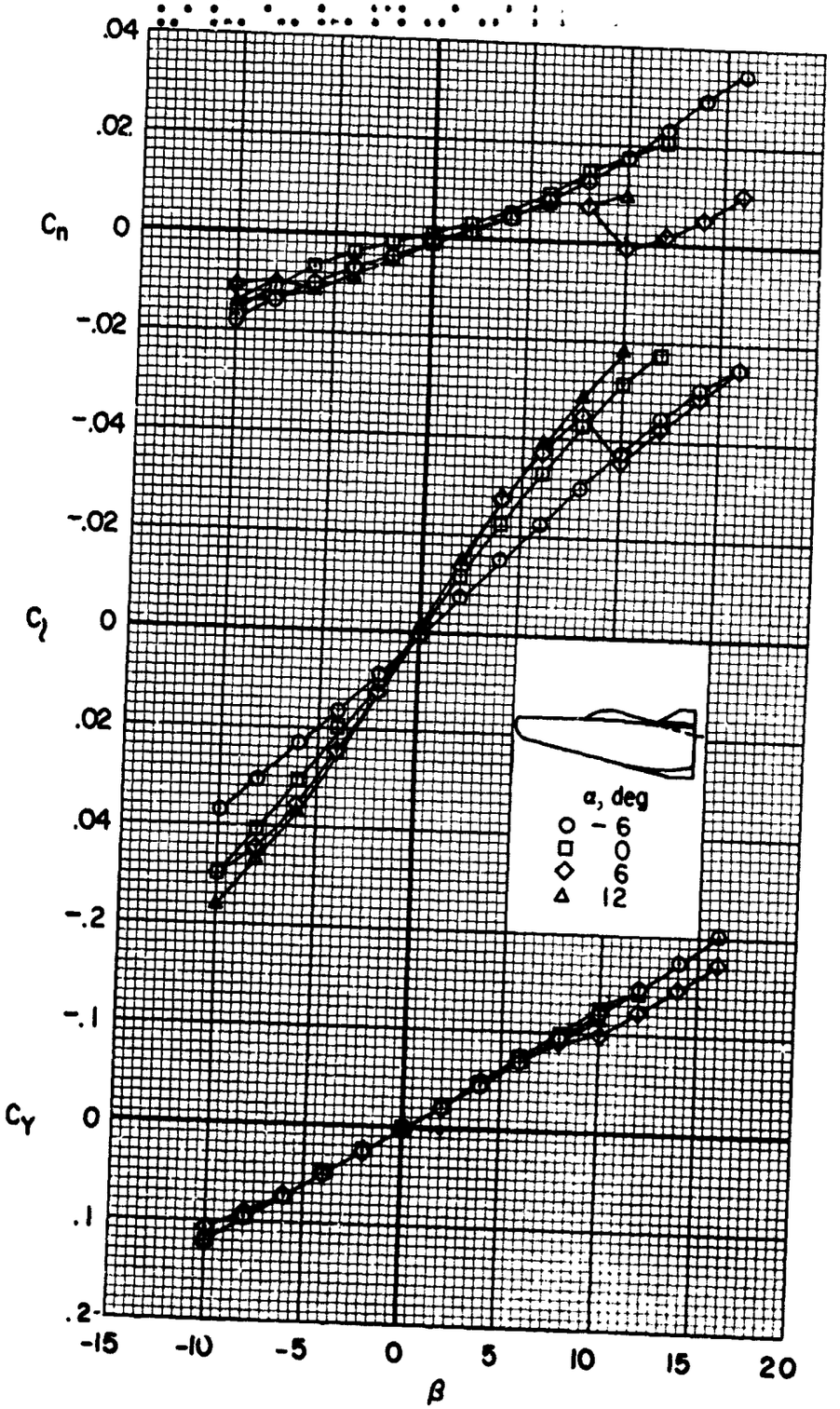

Figure 26.- The lateral and directional characteristics of the complete configuration at several angles of attack; M = 0.25, R = 25×10^6, $\delta_r = -5^\circ$, $\delta_e = 0^\circ$.

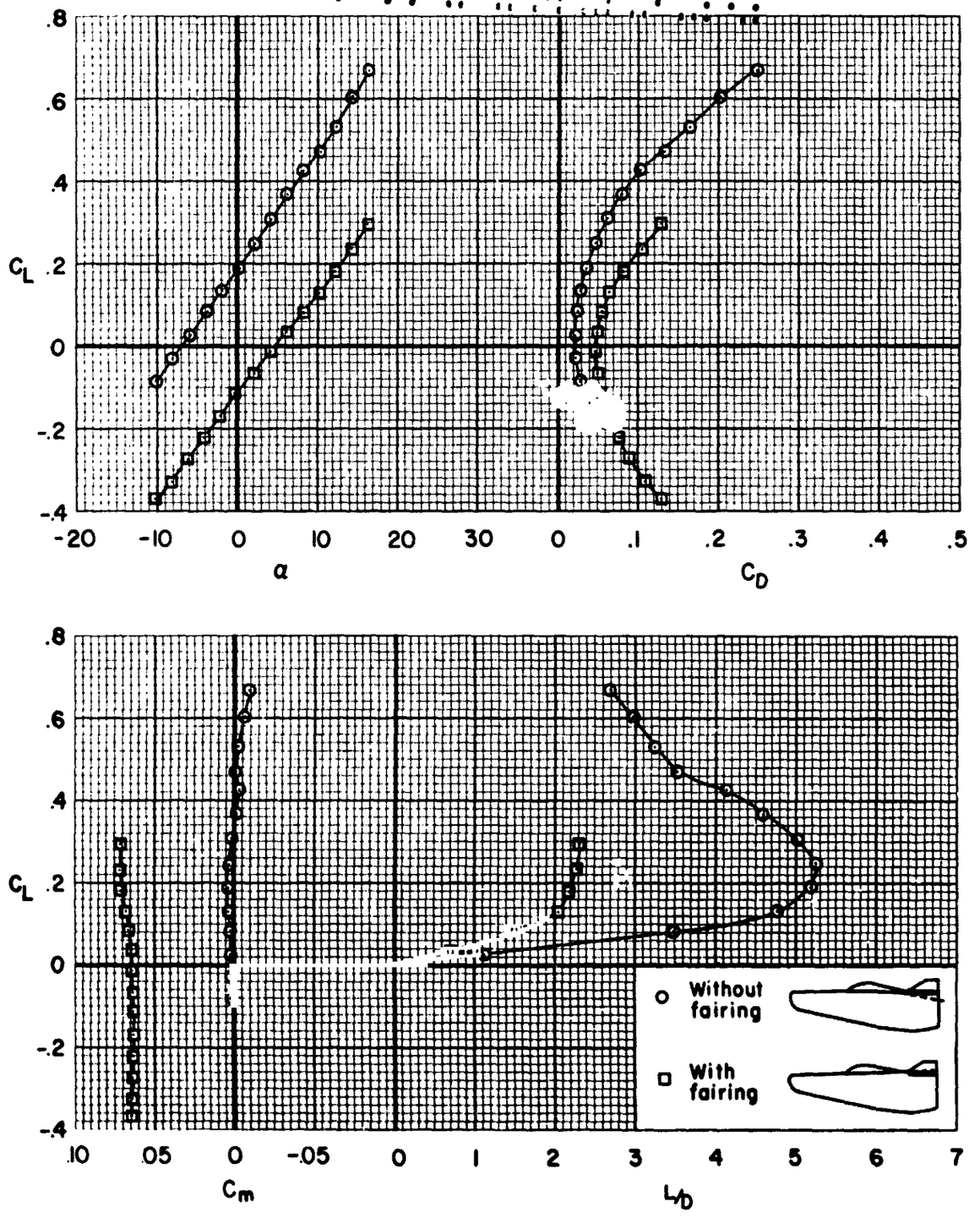

(a) M = 0.60

Figure 27.- The effects of Mach number on the longitudinal characteristics of the complete configuration with and without an upper surface fairing. R = 5×10^6, $\delta_f = -5^\circ$, $\delta_e = 0^\circ$.

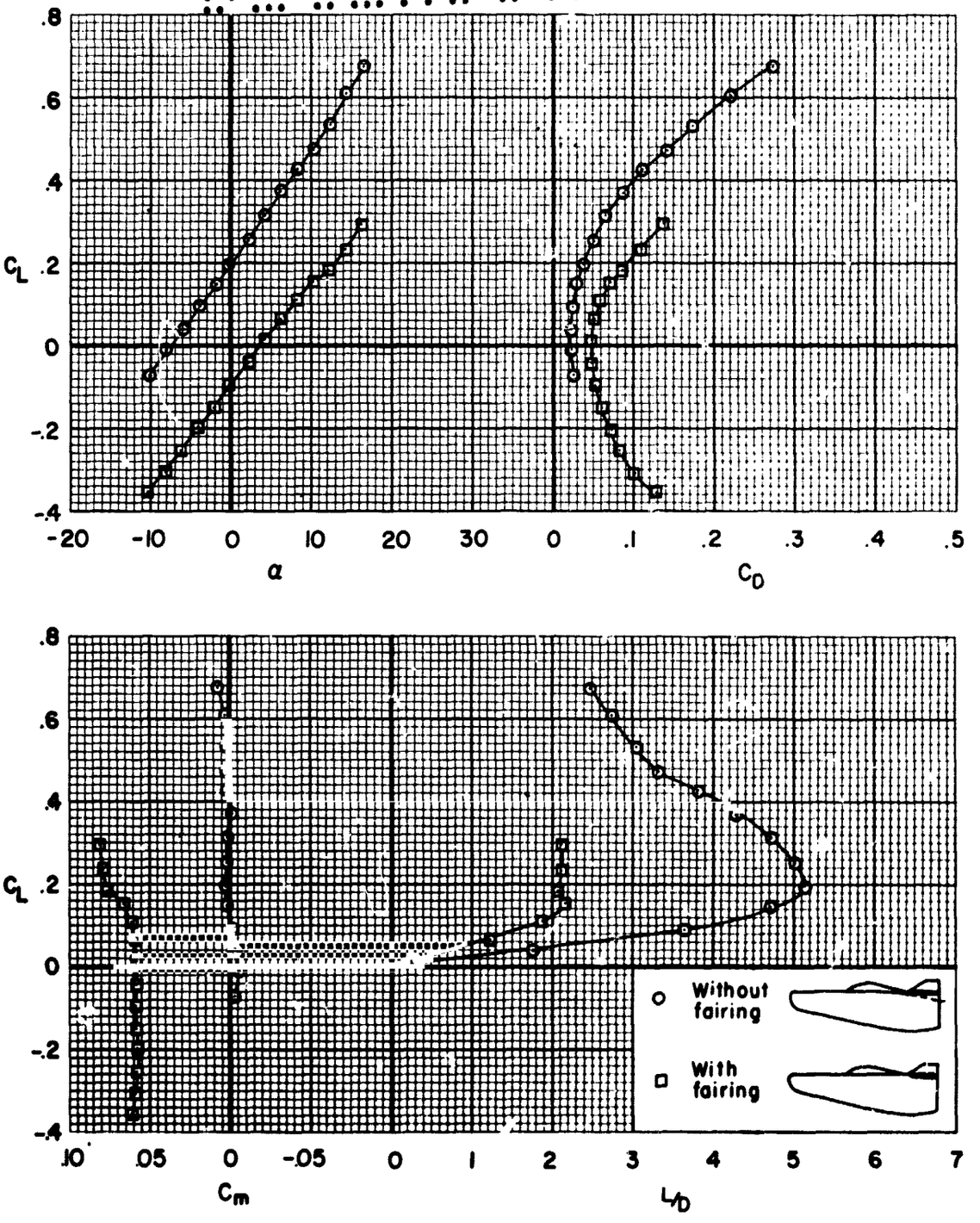

(b) M = 0.70

Figure 27.- Continued.

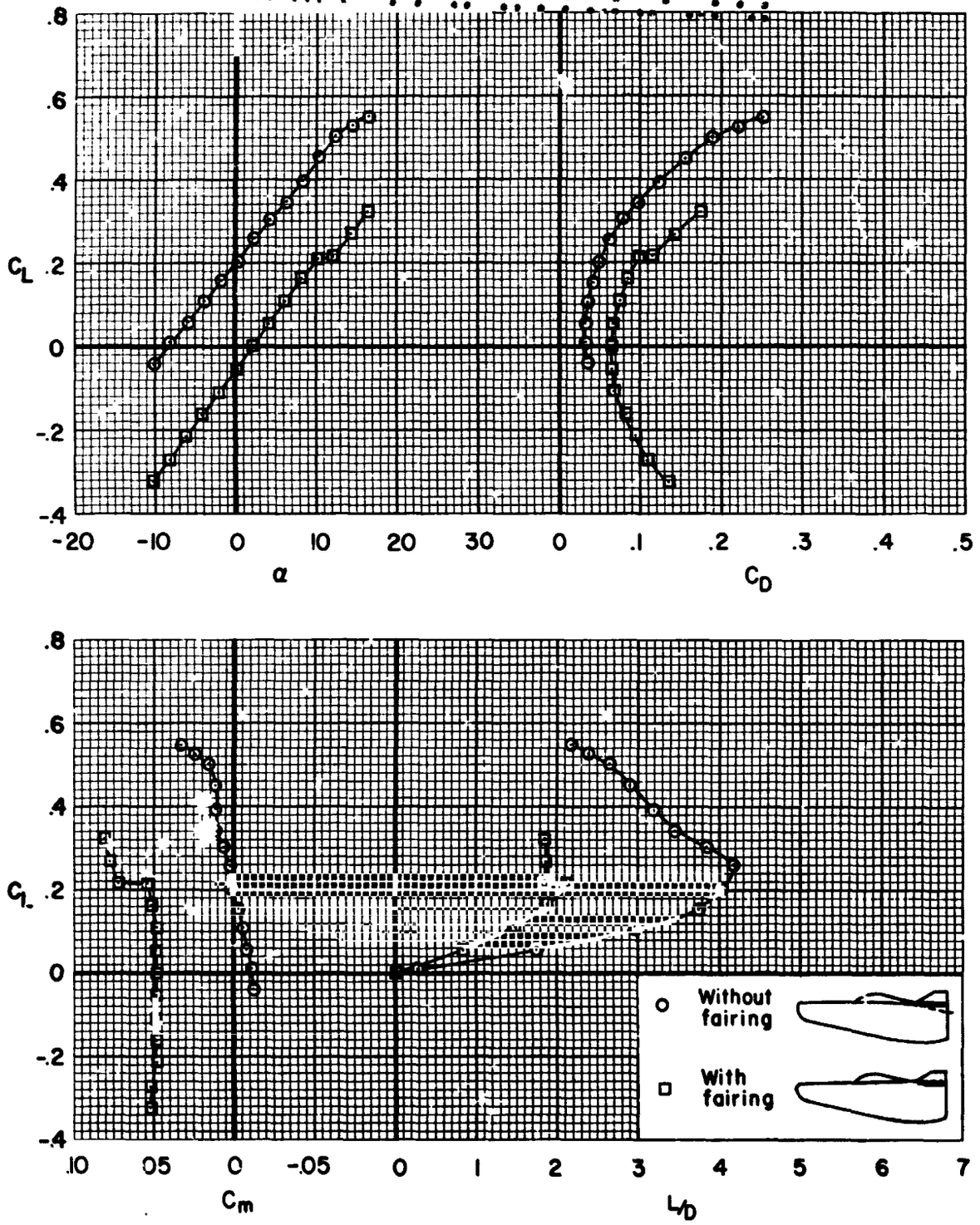

(c) M = 0.80

Figure 27.- Continued.

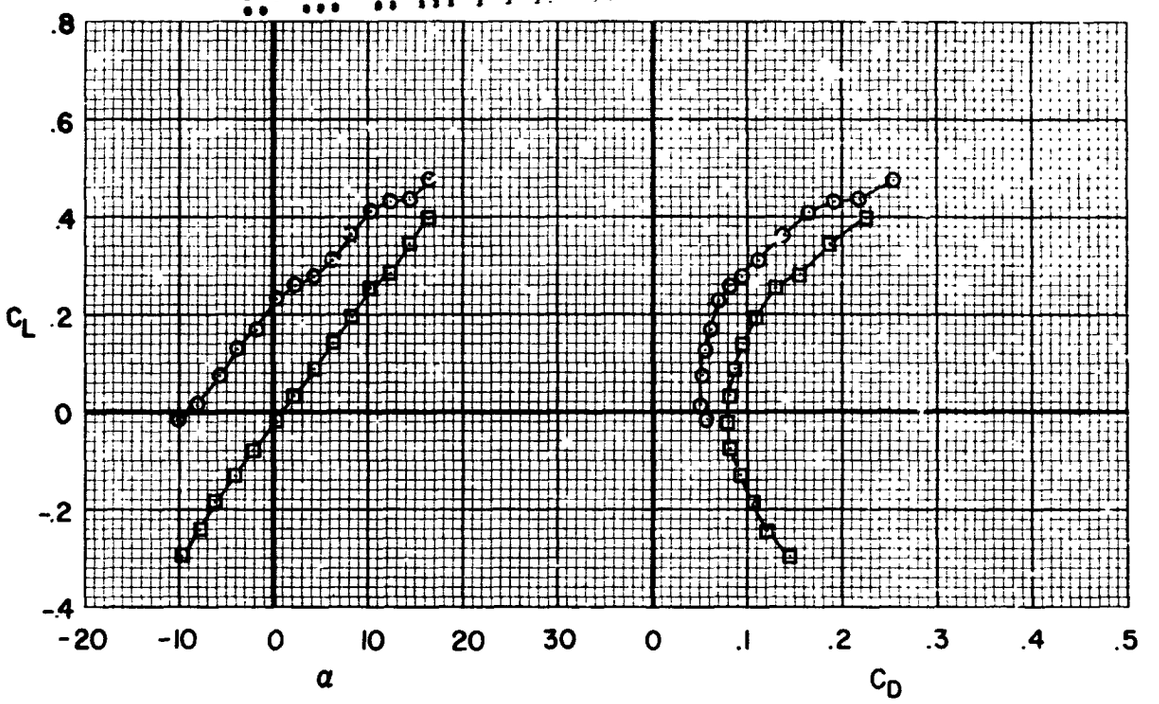

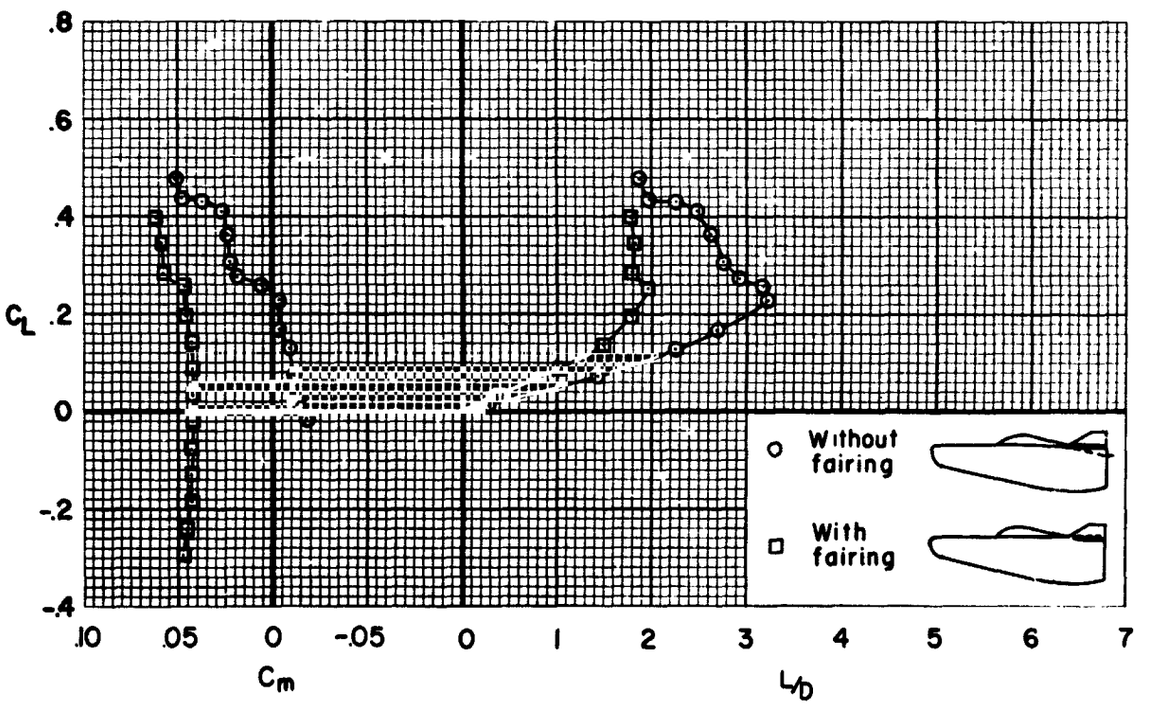

(d) M = 0.85

Figure 27.- Continued.

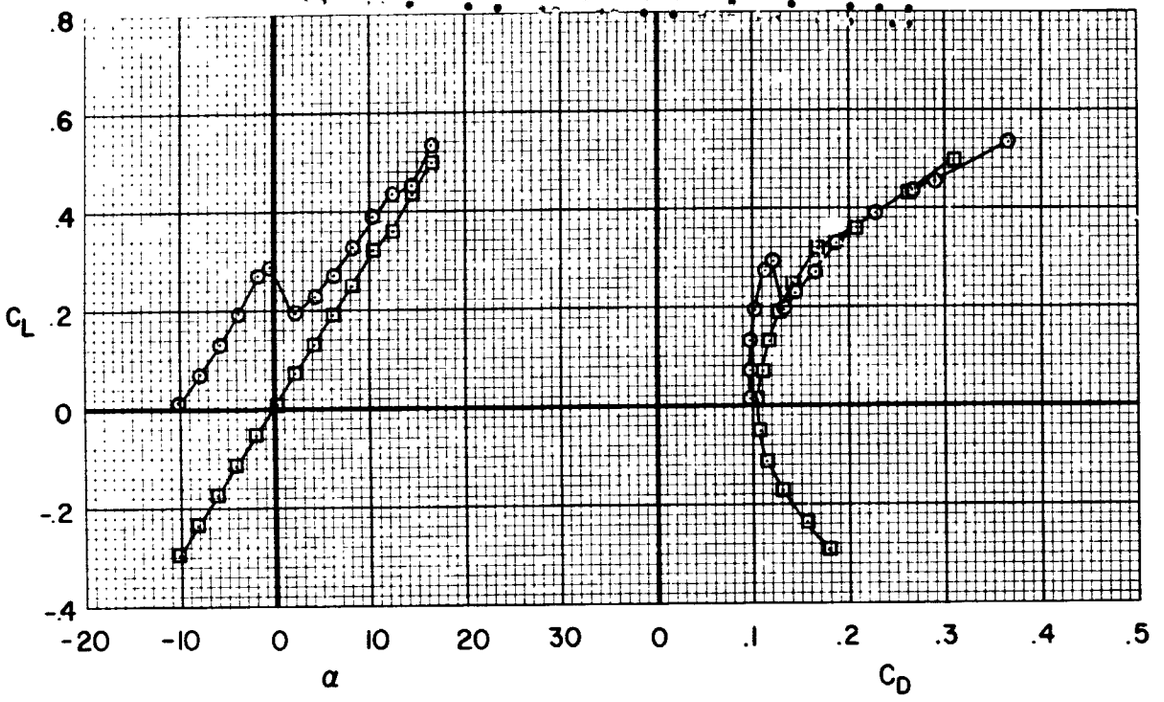

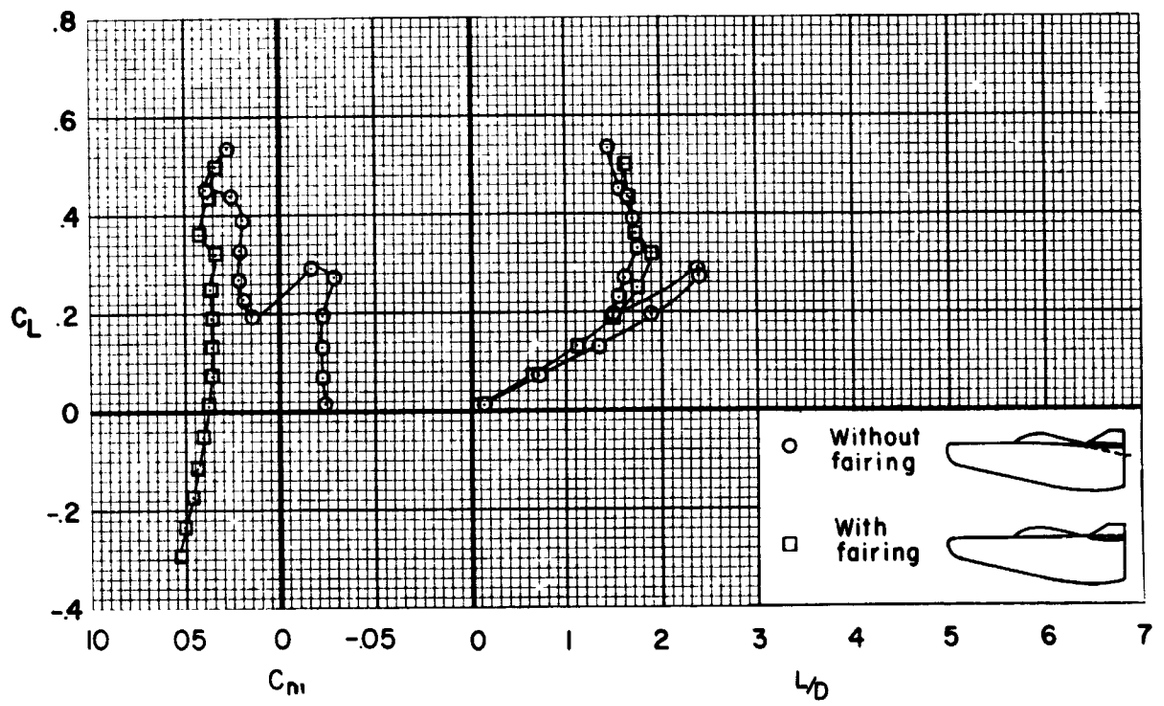

(e) M = 0.90

Figure 27.- Concluded.